JOURNAL OF QUATERNARY SCIENCE (2025) 1–16 ISSN 0267-8179. DOI: 10.1002/jqs.3691

JQS Journal of Quaternary Science QRA Quaternary Research Association

The Pleistocene Witch Ground Ice Stream in the central North Sea

BENEDICT T. I. REINARDY,[1]* JENS KARSTENS,[2] CHRISTOPH BÖTTNER,[2,3] ANNA LICHTSCHLAG,[4] CHRISTIAN BERNDT,[2] NICHOLA A. STRANDBERG[5,6] and BEN J. CALLOW[7]

[1]Department of Sustainable Development, Environmental Science and Engineering, KTH The Royal Institute of Technology, Stockholm, Sweden
[2]GEOMAR Helmholtz-Centre for Ocean Research Kiel, Kiel, Germany
[3]Department of Geoscience, Aarhus University, Aarhus, Denmark
[4]National Oceanography Centre, Southampton, UK
[5]School of Geography and Environmental Science, University of Southampton, UK
[6]The Arctic University Museum of Norway, UiT The Arctic University of Norway, Norway
[7]School of Ocean and Earth Science, University of Southampton, Southampton, UK

Received 26 February 2024; Revised 12 November 2024; Accepted 16 December 2024

ABSTRACT: The North Sea Basin has been covered by ice sheets originating from both the British Isles and Scandinavia at multiple times during the Pleistocene. The Witch Ground Basin (WGB) in the central northern North Sea is a critical location in terms of interpreting Late Pleistocene glacial to glacimarine history of the North Sea since it was the location of the Witch Ground Ice Stream that was active on multiple occasions during the Mid to Late Pleistocene. We map five mega-scale glacial lineation flowsets corresponding to the changing ice flow direction of the Witch Ground Ice Stream and investigate the sedimentological fingerprint and corresponding subglacial depositional processes of this palaeo-ice stream. We show that sorted sand layers within a subglacial traction till represent periodic hydraulic jacking and ice–bed decoupling at the base of the Witch Ground Ice Stream. In contrast to previous studies that have described glacitectonites deposited below the most recent grounded ice in the WGB, we present analysis of sediment cores that recovered primarily massive diamictons without any obvious deformation structures. The most recent ice cover in the WGB (~18–16 ka) was thought to have been sourced from a localized ice cap over Orkney and Shetland. The presence of chalk clasts sourced from NW of the WGB described in this study from the stratigraphically youngest till confirms this interpretation. The transition from subglacial to glacimarine deposition, while acoustically well defined (from opaque to laminated acoustic units), appears surprisingly uniform in the recovered sediment cores, but can be differentiated based on a change in colour including mottling and banding, presence of whole intact shells, and the increased number of silt and sand lenses. ^{14}C dating of glacimarine muds indicate high sedimentation rates of between 80 and 260 cm ka^{-1}. The transition from glacimarine to marine deposition is represented by a comparative decrease in sedimentation rate and deposition of Holocene age sandy mud. This study demonstrates a highly dynamic Witch Ground Ice Stream in the northern North Sea during the Late Pleistocene with evolving subglacial hydrology and depositional processes at the ice stream bed that left a distinct geomorphological and sedimentological fingerprint within the WGB. © 2025 The Authors *Journal of Quaternary Science* Published by John Wiley & Sons Ltd

KEYWORDS: glacimarine; hydraulic jacking; North Sea; palaeo-ice stream; subglacial processes

Introduction

The central and northern North Sea in the vicinity of the Witch Ground Basin (WGB, also known as the 'Fladen Basin' or 'Fladen Ground') has been intensively studied over the last 40 years in relation to the Quaternary glacial history of both the British and Irish Ice Sheet (BIIS) and the Fennoscandian Ice Sheet (FIS) (Fig. 1) (e.g. Sejrup et al., 1987, 1991, 1994, 2015, 2016; Carr et al., 2000, 2006; Graham et al., 2007, 2010; Evans et al., 2021). This is because both ice sheets coalesced in the area at least twice during the Mid to Late Pleistocene and sediments deposited in the WGB correspond to sea level fluctuations, glacial isostatic adjustment of the North Sea Basin, and the interaction of the North Atlantic with the marine-based sectors of both the BIIS and FIS (Graham et al., 2011). Ice sheet geometry within the northern North Sea evolved during multiple glacial cycles in the Mid to Late Pleistocene with BIIS and FIS ice build-up, maximum ice extent along the continental shelf edge and subsequent deglaciation (e.g. Reinardy et al., 2017). Either throughout or at certain times within these glacial cycles, grounded ice along this sector of the North Sea was drained by the Witch Ground Ice Stream (Graham et al., 2007, 2010). Thus, the area around the WGB appears to have experienced a complex history of ice retreat and advance coupled with the Witch Ground Ice Stream that existed during multiple periods throughout the Mid to Late Pleistocene. While the Witch Ground Ice Stream has been identified based on geomorphological mapping of mega-scale glacial lineations (MSGLs), it is still unclear what glaciological controls and mechanisms caused ice streaming within the WGB. In context of the BIIS, this question is not unique to the Witch Ground Ice Stream. Similar questions have been posed for the neighbouring North Sea Lobe ice stream, the Minch Ice Stream and the Irish Sea Ice Stream (Gandy et al., 2018; Roberts et al., 2018b; Scourse et al., 2021). These studies have focused on modelling and geomorphological evidence to suggest non-steady-state oscillations or

*Correspondence: Benedict T. I. Reinardy, as above.
Email: reinardy@kth.se

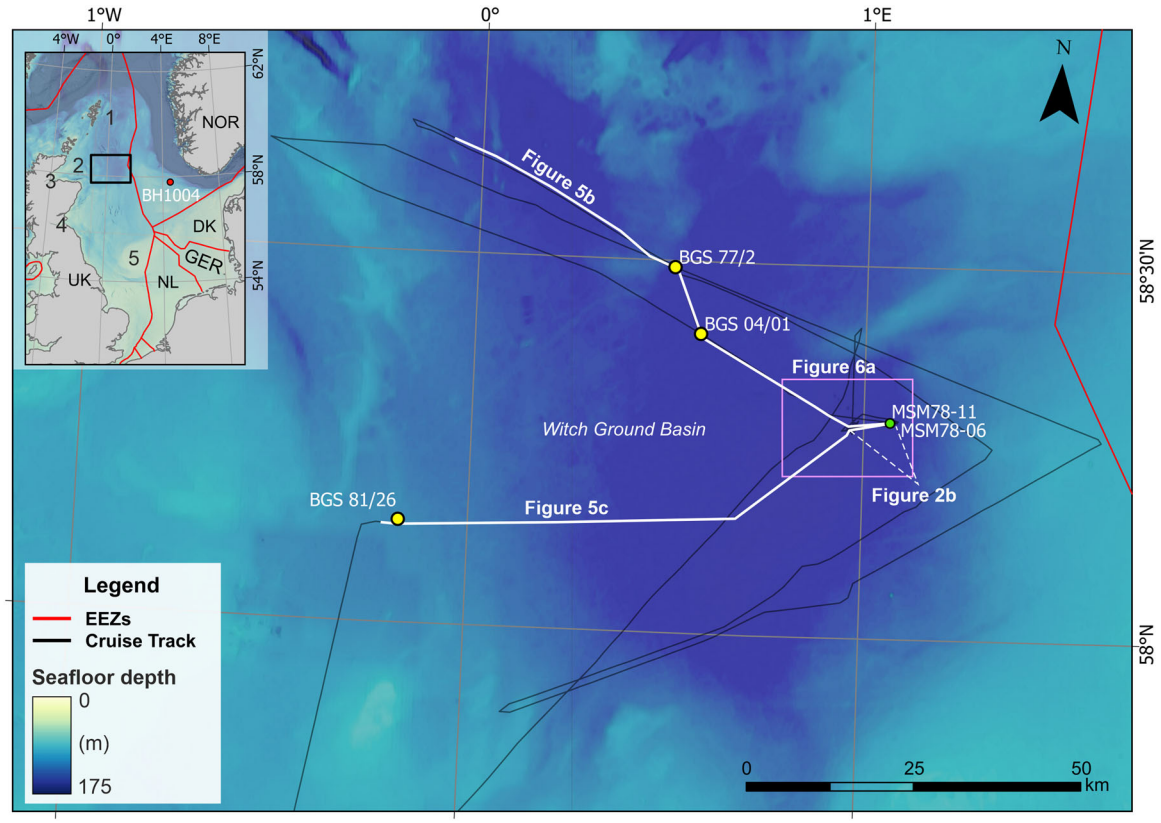

Figure 1. Seafloor bathymetry of the Witch Ground Basin, central North Sea, supplied by EMODnet. Ship track lines of cruise MSM78 are indicated (black lines) including track lines along which echosounder data were collected (white lines) and displayed in Figs. 2(C) and 5. The map shows the borehole site where MSM78-11 and MSM78-06 were collected (green dot) during cruise MSM78. Also included are borehole sites from the British Geological Survey (BGS) (yellow dots) discussed in the main text and location of the amplitude map displayed in Fig. 6(A) (pink box). The inset shows the location of the survey area (black box) within the North Sea. The red dot marks the location of borehole BH1004 on the Egersundbanken. The red line shows national boundaries. Various locations discussed in the main text are numbered: 1 = Pobie Bank; 2 = Bosies Bank; 3 = Moray Firth; 4 = Firth of Fourth; and 5 = Dogger Bank. [Color figure can be viewed at wileyonlinelibrary.com]

surges of these ice streams possibly driven by changes or instabilities of the basal hydrological system, which in turn would have influenced basal lubrication and subglacial flow processes (e.g. Clark et al., 2022). Here, we aim to investigate the geomorphological and sedimentological fingerprint and corresponding subglacial to ice-marginal glacimarine depositional processes of the Witch Ground Ice Stream and consider the wider glaciological implications for this and other marine-based sectors of the BIIS. To achieve this, we investigated 3D seismic data along with recently collected parametric echosounder data as well as cores and radiocarbon dating to provide a stratigraphic framework for the recovered sediments. Echosounder data were specifically collected to stratigraphically link the results from the cores described here with those from previous studies based on British Geological Survey (BGS) borehole sites within the WGB (Fig. 1).

Previous work on the Mid to Late Pleistocene glacial history of the WGB

The age of both the sedimentary and geomorphic evidence relating to ice advance and retreat in the WGB during the Mid to Late Pleistocene is still debated, but there is good evidence for the presence of extensive ice cover in the central North Sea during Marine Isotope Stage (MIS) 6 and MIS2 and possibly also MIS4 (Graham et al., 2011; Batchelor et al., 2019). There is good agreement in the maximum extent of ice cover during MIS2 at the Last Glacial Maximum (LGM; ~26–21 ka) when the BIIS and FIS coalesced in and around the WGB (Bradwell et al., 2019; Clark et al., 2022). Cores from the WGB have recovered sequences of diamicton, interpreted as till and glacimarine sediments deposited at and/or proximal to the grounding line as well as grounding line distal deposits including marine mud dated to the Late Pleistocene (e.g. Sejrup et al., 1987, 2015). Multiple subglacial bedforms exist both at the seafloor and within the uppermost Late Pleistocene sedimentary sequences within the WGB. These include moraines, grounding zone wedges, MSGLs and meltwater channels sometimes in the form of tunnel valleys around the margins of the WGB (Graham et al., 2007, 2010; Bradwell et al., 2019; Evans et al., 2021; Kirkham et al., 2021). Debris flow deposits and multiple iceberg-scoured surfaces within the Late Pleistocene sedimentary sequences correspond to glacimarine conditions during which time the extent of grounded ice in the North Sea is more speculative (Haavik and Landrø 2014; Newton et al., 2024).

The timing of coalescence of the BIIS and FIS during MIS2 as well as deglaciation after the LGM in the WGB is debated in large part because there may have been multiple readvances or oscillations of the ice margin (discussed below) during overall deglaciation of the northern North Sea, a style of retreat that is not uncommon among other palaeo-ice sheets (e.g. Callard et al., 2020; Funder et al., 2021). These readvances may have been driven by neighbouring changes in North Atlantic circulation, and changes in sea level and/or the dynamics of the Norwegian Channel Ice Stream to the east and the Firth of Forth/Moray Firth ice streams to the west (Fig. 1) (Evans et al., 2021; Sejrup et al., 2021). Ice streams play a fundamental role in the mass balance of ice sheets, and evidence of palaeo-ice steams, primarily sets of MSGLs, exists across the Norwegian Channel and the central and northern part of the North Sea (Ottesen et al., 2014; Svendsen et al.,

2015; Buckley 2017; Morén et al., 2017; Reinardy et al., 2017). Graham et al., (2007, 2010) mapped four 'flowsets' of MSGLs within the WGB formed at the base of the Witch Ground Ice Stream at different times throughout the Mid to Late Pleistocene. Flowsets 1 (stratigraphically lowest) and 2 were interpreted as MIS6–MIS4 in age with ice flow from the southwest to northeast (Graham et al., 2011). Flowsets 3 and 4 (stratigraphically highest) were interpreted as MIS2 in age. Flowset 3 was linked to the most extensive ice cover in the North Sea during MIS2, e.g. the LGM with ice flow sourced from the southeast and flowing to the northwest. The stratigraphically youngest MSGL (Flowset 4) is thought to correspond to localized ice over Shetland and Orkney flowing southeast to the WGB, possibly related to surging of the ice margin in this area (Evans et al., 2021). Diamictons interpreted as tills have also been correlated to ice advance during MIS2, MIS4 and MIS6 based on limited chronological constraints (Sejrup et al., 1987, 1991, 1994, 2015, 2016; Carr et al., 2000, 2006; Graham et al., 2007, 2010; Evans et al., 2021).

Since the arrival of high-resolution swath bathymetry covering most of the North Sea, the maximum extent of ice during the LGM in MIS2 has been relatively well defined by sequences of ice-marginal moraines indicating coalescence of the BIIS and FIS and ice advance to the continental shelf edge (Dove et al., 2017; Roberts et al., 2018a; Bradwell et al., 2019). What is still debated is the exact timing of maximum ice cover and the timing, rate and pattern of proceeding ice retreat from the North Sea and in particular the central North Sea around the WGB. Hughes et al. (2016) suggest coalescence of the BIIS and FIS between ~27 and 22 ka, while Bradwell et al. (2019) and Clark et al. (2022) indicate a slightly shorter period from 26 to 22 ka. Sejrup et al. (2016) suggest maximum ice cover from 23 to 19 ka while based on ice sheet models Patton et al., (2016, 2017) suggest a very short period of coalescence between 23 and 22 ka.

Clark et al. (2022) and Gandy et al. (2021) suggest initial deglaciation of the northern North Sea started at 21 ka, initiated by retreat of the Norwegian Channel Ice Stream although retreat of the Norwegian Channel Ice Stream from the continental shelf edge has been dated slightly later between 20 and 19 ka (Svendsen et al., 2015; Morén et al., 2017). This led to the separation of the BIIS and FIS along the western margin of the Norwegian Channel and rapid inundation of the WGB by marine waters possibly already at around 20 ka (Bradwell et al., 2008; Evans et al., 2021). The WGB is an area of relatively deep water (>140 m) compared to the rest of the North Sea (excluding the Norwegian Channel) and would be the first area to become inundated with marine waters as the BIIS and FIS separated and retreated from the continental shelf edge. This in turn would have led to the expansion of calving margins possibly within a calving bay (Sejrup et al., 1987; Bradwell et al., 2008; Graham et al., 2010; Merritt et al., 2017; Gandy et al., 2021). The corresponding ice sheet model reconstruction of Clark et al. (2022) suggests streaming ice flowing into a large calving bay in the vicinity the WGB. Further deglaciation of the northern North Sea was oscillatory, driven by significant reordering of the configuration of ice flow, with readvances of ice sourced from a localized Shetland–Orkney ice cap (Bradwell et al., 2019; Evans et al., 2021). By 18.7 ka, the Norwegian Channel Ice Stream had retreated southeast of the WGB which possibly led to the drainage of a large proglacial lake from the southern North Sea through the Ling Bank drainage channel directly west of the WGB (Hjelstuen et al., 2018). An independent Shetland Ice Cap had formed by 18 ka which further separated from grounded ice on the continental shelf to the east at 17 ka forming the short-lived Pobie Bank Ice Cap which had gone by 16 ka (Clark et al., 2022). During this time two readvances of ice depositing moraines at the northern margin of the WGB have been identified, the Fladen 1 (18–17.4 ka) and Fladen 2 (16.3 – 15.2 ka) events (Sejrup et al., 2015; Evans et al., 2021). These ice readvances are thought to have been sourced from the northwest possibly related to the localized ice caps on Shetland and Pobie Bank (Fig. 1) (Sejrup et al., 2015). While these readvances are rather late within the overall deglaciation chronology on the North Sea Basin, they do approximately correspond to Heinrich Stadial 1 (16.8–14.7 ka), during which time sea ice was present in the North Atlantic south of Iceland (Thornalley et al., 2011) and fit with a deglaciation age of 15 ka for the Bosies Bank moraine complex to the northwest of the WGB (Fig. 1) (Evans et al., 2021). One possible explanation for the complex chronologies may relate to local ice, possibly in shallow waters to the east of Shetland, surviving until relatively late in the overall deglaciation of the shelf (Bradwell et al., 2019). Another possibility suggested by Evans et al. (2021) is that the readvances of Fladen 1 and 2 represent surge-type behaviour in this sector of the ice margin after initial ice retreat back to the vicinity of Orkney and Shetland, similar to several other sectors of the BIIS that surged after initial retreat (Gandy et al., 2018; Roberts et al., 2018b; Scourse et al., 2021).

Seafloor morphology in and around the Witch Ground Basin

The seafloor morphology of the WGB has been extensively mapped and described elsewhere (e.g. Bradwell et al., 2008, 2019; Evans et al., 2021). Here, we provide a concise description of this previous work to provide context to our new mapping. The WGB forms the southern extent of a larger basin that is below 100 m water depth and is bounded by the continental shelf edge to the north, the Shetland and Orkney islands to the west, and the Norwegian Channel to the east (Fig. 1). The central WGB seafloor is characterized by a flat and smooth seafloor topography at the regional scale, contrasting with distinct ridges and mounds to the north and south. These features are interpreted as ice-marginal moraines, grounding zone wedges and debris flow lobes. Branching and anastomosing channels, extending northwestward from the WGB, reach depths of tens of metres and span up to 30 km in length. These channels are occasionally partially filled with sediment. These channels also start and end abruptly and have undulating thalwegs and have thus been interpreted as tunnel valleys.

Within the WGB, abundant depressions occur in water depths between 120 and 180 m over an area 225 km^2 and have been interpreted as pockmarks (Fig. 2a, b) (Judd et al., 1994; Gafeira et al., 2018; Böttner et al., 2019). Pockmarks vary in size from 5 to 180 m in diameter and 1 to 16 m in depth (Fig. 2c). The density and shape of these pockmarks change according to glacial and postglacial sediment distribution and thickness within the WGB, indicating a strong dependency on the hosting sediments. In areas where till crops out at seafloor, pockmarks are absent, but are rather preferentially located within areas of thick (>5 m) glacimarine and marine sediments. The elongated shapes of the pockmarks show distinct strike directions, which may be attributed to local bottom currents reshaping the seafloor (Fig. 2b). Where pockmarks are absent, the seafloor is characterized by linear and curvilinear depressions, which have been interpreted as iceberg scour marks.

Methods

Swath bathymetric and echosounder data along with sediment cores were collected in the WGB during cruise MSM78

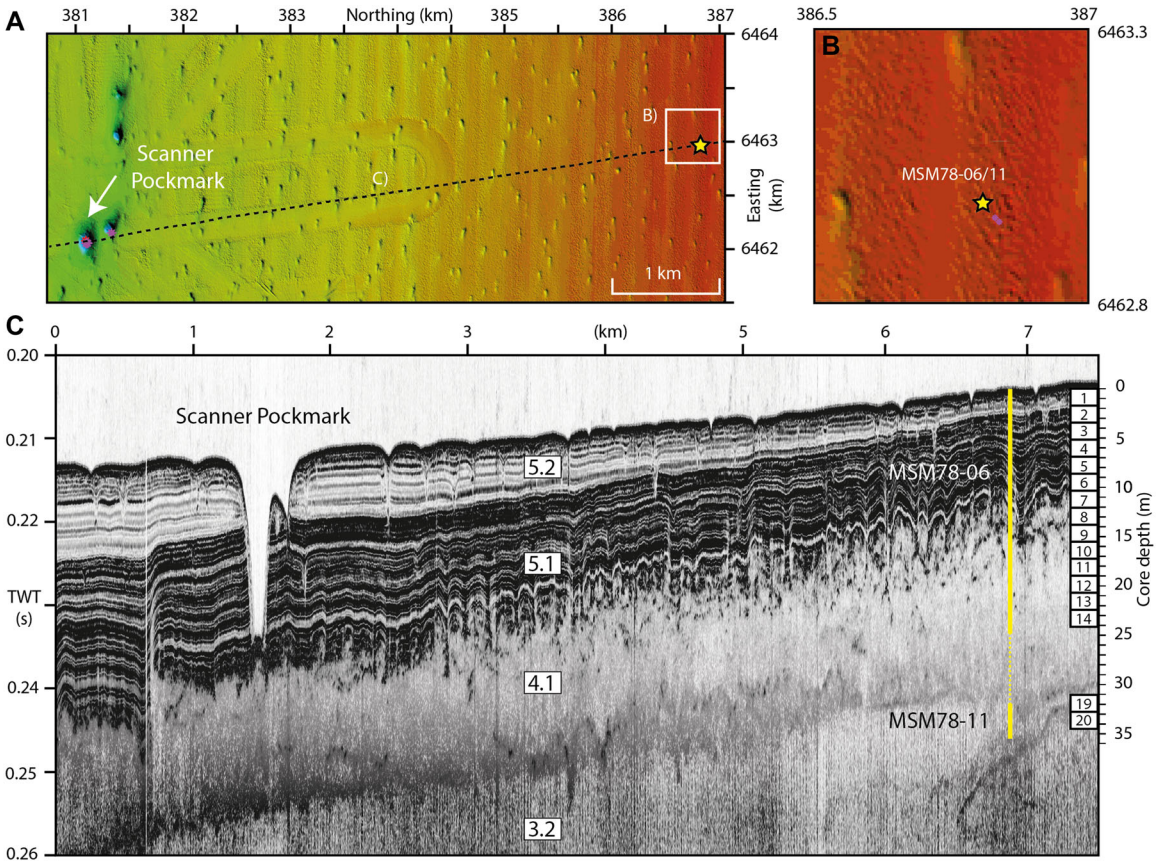

Figure 2. Seafloor bathymetry showing numerous pockmarks around the borehole site of cores MSM78-11 and MSM78-06. White square is seafloor area shown in detail in (B) in the vicinity of the MSM78-11 and MSM78-06 borehole site. The dashed black line in (A) indicates the location of the parasound profile displayed in (C) from MSM78-11 and MSM78-06 borehole site towards the Scanner pockmark. The location of the parasound profile within a regional context is shown in Fig. 1. Labels 3.2, 4.1, 5.1 and 5.1 correspond to acoustic units. Numbered boxes 1–20 on the right of the profile correspond to core sections. [Color figure can be viewed at wileyonlinelibrary.com]

onboard RV *Maria S. Merian* during October 2018 (Figs. 1 and 2). Bathymetric data were acquired with a hull-mounted EM712 system. The survey was designed to provide high-resolution bathymetry with 5 × 5-m resolution. Data processing and gridding of the EM712 data was carried out onboard using the MB Systems software package Version 5.5.2303 (release: 28 April 2017). The gridding was performed using a Gaussian weighted mean with a cell size of 15 m. To eliminate unwanted influence of outer beams on the grid induced by deviation of the outer beams, we applied a spline tension with a value of 2. All data were interpolated for a maximum of three cell sizes to achieve good coverage for the high-resolution grid. The sound velocity profile for multibeam processing was measured at the beginning and at the end of the cruise. The shallow seismic stratigraphy was imaged by subbottom profiler (SBP) data acquired using a Parasound P70 with 4 kHz as the secondary low frequency to obtain seismic images of the upper 50–100 m below the seafloor with very high vertical resolution (<15 cm) (e.g. Fig. 2c). Due to the shallow water depth (<200 m) in the WGB, the P70 system was operated in a single pulse mode. We applied a frequency filter (low cut 2 kHz, high cut 6 kHz, two iterations) and calculated the envelope within the seismic interpretation software IHS Kingdom. We used a velocity of 1700 m s^{-1} as suggested by Ottesen et al. (2014) based on information from a series of wells across the North Sea, for depth conversion purposes. We used these depth calculations to select locations for the BGS RockDrill2. Alongside the echosounder data, we used an extensive 3-D industry pre-stack time-migrated seismic amplitude data set 'CNS MegaSurvey' provided by TGS that covers >22 000 km^2 of the central to northern North Sea down to 1.5 s two-way travel time (TWT). The quality of this data set is variable due to different acquisition and processing techniques involved in the different cubes but the vertical resolution is ~20 m with an inline and crossline spacing of 12.5 m. We used seismic amplitude maps to enhance seismic interpretation of regionally extensive subglacial bedforms (e.g. MSGLs).

During cruise MSM78, the RockDrill2 was deployed in the WGB in the vicinity of the Scanner pockmark and ~5 km to the west of the pockmark, which is the focus of this study (Figs. 1 and 2a, b). The RockDrill2 is a remotely operated multi-barrel wireline subsea robotic sampling system, launched from its own Launch and Recovery System (LARS). Continuous 1.72-m core sections are taken using an internal core barrel, which is recovered through the main drill string with a wireline system. This means that the depth of the individual core barrels below seafloor is known and increases in 1.7-m increments. However, recovery of sediment within individual core barrels was never 100% and often around 70% (Fig. 2c). Thus, for each core barrel and corresponding core section we assumed that the top of the core section corresponded to the top of the core barrel and used this to log the depth below seafloor of each core section. The core section is then stored in the drill tool rack, subsea, until the target depth has been achieved. A significant advantage with the RockDrill2 system over many conventional coring systems is the ability to core consolidated diamicton, common in formally glaciated terranes. Two boreholes were drilled at the site west of the Scanner pockmark (Fig. 2a, c). MSM78-06 was drilled in 149 m water depth, consisting of 14 sections extending from the seafloor down to 24.14 m below seafloor (mbsf) and an average core recovery of 70% (Figs. 2c and 3). MSM78-11 was drilled in

Table 1. One- or two-centimetre-long samples from MSM78-11 and MSM78-06 sieved for shell material on which radiocarbon measurement were made. The AMS ^{14}C dates were converted to calendar age (cal a BP) using the Marine20 calibration curve of Heaton et al. (2020).

Core	Lab. no.	Depth below seafloor (m)	Acoustic unit	Depositional environment	^{14}C age (BP)	Calibrated calendar age (cal a BP)
MSM78-06	Poz-136940	3.95–3.97	5.1	Glacimarine	11 450 ± 70	12 750 ± 70
MSM78-06	Poz-136941	12.44–12.45	5.1	Glacimarine	23 160 ± 170	26 470 ± 170
MSM78-06	Poz-136942	18.91–18.93	4.1	Subglacial	>51 000	
MSM78-06	Poz-136943	21.07–21.09	4.1	Subglacial	>50 000	
MSM78-06	Poz-136944	22.65–22.66	4.1	Subglacial	>46 000	
MSM78-11	Poz-136945	32.77–32.79	3.2	Subglacial	44 000 ± 2 000	45 600 ± 2 000
MSM78-11	Poz-136946	32.9–33	3.2	Subglacial	>50 000	

160 m water depth, consisting of two sections extending down from 32 to 35.44 mbsf (the upper 32 m was drilled as an open borehole), but with an average core recovery of only 30%.

Cores were split into working and archive halves using a GEOTEK core splitter and piano wire. After cleaning the core surface, the archive half was imaged with a high-resolution Geoscan IV camera as soon as possible to avoid sediment colour changes caused by oxidation and drying (Fig. 4). Colour was recorded using a Munsell soil colour chart. Microscopic descriptions from smear slides were taken in a majority of core sections, but in particular where slight changes in lithology were thought to occur, i.e. from clayey silt to silty clay. Biogenic remains were also identified in smear slides.

Thirteen half core samples were taken from MSM78-06 and four half core samples from MSM78-11. Each half core sample was 1–2 cm thick and was used for sieving to extract shell material on which to carry out accelerator mass spectrometry (AMS) radiocarbon dating (Table 1). Sampling intervals targeted areas with macroscopically visible shell fragments, but also covering depth intervals that corresponded to each acoustic unit (S3.2–S5.2). Of the 13 samples from MSM78-06, five had >20 mg of shell material, either mollusc shell fragments or foraminifera shells, while two of the four samples from MSM78-11 had the required volume (>20 mg) of shell material, in this case mollusc shell fragments. Samples were then sent to the Poznan Radiocarbon Laboratory and underwent (i) chemical pre-treatment, (ii) production of CO_2 and graphitization, (iii) AMS ^{14}C measurement calculation of ^{14}C age and (iv) calibration of ^{14}C age. Full details of sample treatment and laboratory procedures can be found in Goslar (2015). The AMS ^{14}C dates were converted to calendar age (cal a BP) using the Marine20 calibration curve of Heaton et al. (2020).

Results

Acoustic stratigraphy

The full Quaternary acoustic stratigraphy that is close to 1 km thick in the WGB has been previously described (e.g. Ottesen et al., 2014, 2018; Reinardy et al., 2017; Newton et al., 2024) and here we focus on the detailed near-surface (<40 mbsf) stratigraphy of Mid to Late Pleistocene age (Figs. 2c and 5). The uppermost 40 m of echosounder data show four acoustically distinct units, S3.2 (oldest) to S4.2 (youngest). Unit S3.2 is chaotic to transparent with laterally discontinuous weak and planar to gently dipping reflections towards the top of the unit. The upper boundary of S3.2 is faint, indistinct and highly irregular (Fig. 2c). S4.1 is also chaotic to transparent but contains occasional laterally discontinuous irregular reflections of variable strength. Towards the top of S4.1 these reflections become stronger just below the sharp, corrugated upper boundary separating S4.1 and S5.1 (Fig. 2c). The lower part of S5.1 (~15–13 mbsf) contains laterally discontinuous laminations, but a majority of S5.1 (~13–2.5 mbsf) consists of laterally continuous, very well-laminated reflections with high-amplitude responses (Fig. 5). V-shaped amplitude anomalies at specific stratigraphic horizons in S5.1 correspond to small (in comparison to Scanner) pockmarks (Fig. 2c) (cf. Böttner et al., 2019). A sharp, continuous, planar to wavy boundary separates S5.1 and the uppermost acoustic unit S5.2. S5.2 (~2.5–0 mbsf) is very similar to S5.1 in that it contains well-laminated laterally continuous reflections, but with much lower amplitudes (Figs. 2c and 3). Again, small pockmarks are picked out from V-shaped amplitude anomalies. Both S5.1 and S5.2 show local vertical amplitude discontinuities, possibly indicating fractures in the subsurface. The 3D seismic data were used to calculate seismic amplitude maps at corresponding depths to the acoustic units. From the amplitude maps we identified five MSGL flowsets across the WGB between 10 and 40 mbsf (Fig. 6a). We have numbered flowsets 1 (oldest) to 5 (youngest) according to relative age based on stratigraphic position and cross-cutting relationship where resolution allows.

Core sedimentology and chronology

The lowermost section of MSM78-11 recovered sediments between 34.17 and 33.72 mbsf, while the second section recovered sediments between 32.46 and 32 mbsf (Fig. 3). These sediments correspond to acoustic unit S3.2. Both sections contained a dark grey very stiff mud (Fig. 4a), slightly stiffer and sandier in the lowest section, with some shell fragments and rare isolated clasts. We have described these sediments as 'stiff' based on the comparatively soft marine sediments at and just below (<2 m) the seafloor.

MSM78-06 was drilled down to 24.14 mbsf and penetrated three acoustic units, from bottom up S4.1, S5.1 and S5.2 (Fig. 3). While acoustically these units appear very different in character, overall, the sedimentary characteristics of the 14 core sections of MSM78-06 were remarkably similar although downcore variation in colour, texture and structure were observed (Fig. 4). The sediment between 23 and 15 mbsf (corresponding to unit S4.1) consists of stiff, grey silty clay with shell fragments and occasional faint black mottling (Fig. 4b, c). The silty clay is slightly lighter in colour and less stiff compared to the stratigraphically lower, previously described dark grey very stiff mud (S3.2) recovered in MSM78-11. The most distinct features are sand layers within the silty clay from 1 to 23 cm thick with planar and/or dipping and/or wavy upper and lower boundaries (Fig. 4c). The stratigraphically lowest sand layer occurs at the base of core MSM78-06 (~23 mbsf), is 11 cm thick and contains chalk fragments <1 cm in size (Fig. 4b). Two medium sand size layers between 22 and 21 mbsf are massive, the stratigraphically lowest is non-planar

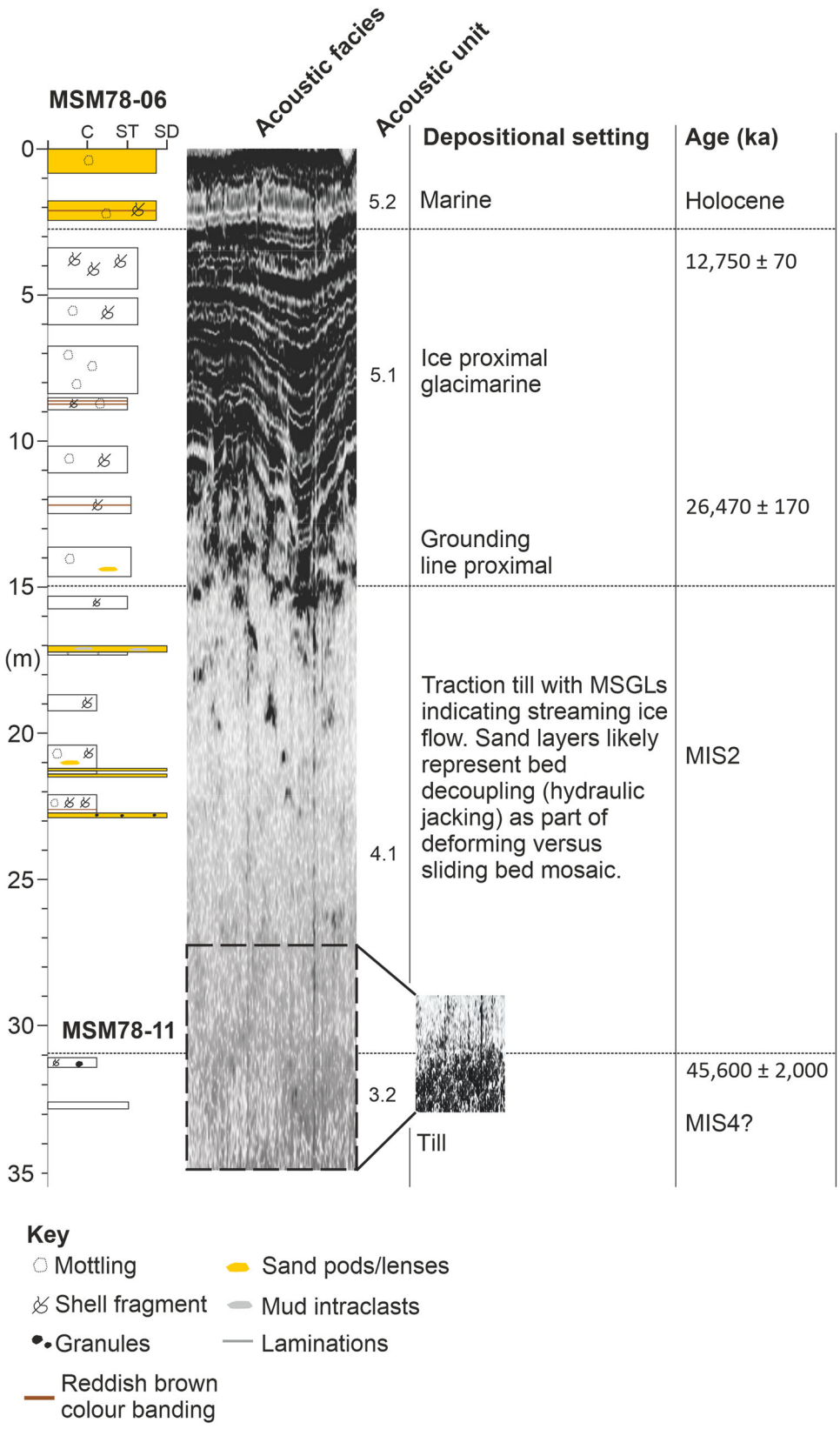

Figure 3. Core logs of MSM78-06 and MSM78-11 with corresponding acoustic stratigraphy from the borehole site. The displayed acoustic profile extends 200 m on either side of the borehole site in a west (left) to east (right) orientation. The contrast of the acoustic facies has been adjusted and displayed to the right to highlight the boundary between S3.2 and S4.1. [Color figure can be viewed at wileyonlinelibrary.com]

and 6.5 cm thick and the upper sand layer is 1 cm thick and planar (Fig. 3). The uppermost sand layer (~17 mbsf) is 23 cm thick and planar but occurs at the core top of core section 11 and may well be thicker (Fig. 4c). In addition, what appear to be mud inclusions are probably caused by drilling disturbance.

From ~15 to 2.5 mbsf (S5.1) is similar to the lower half of the core with primarily stiff, massive silty clay although overall is marginally coarser with higher silt and/or fine sand content and grey brown in colour (Figs. 3 and 4d). Fine sand is occasionally concentrated into pods or lenses. Shell fragments, rare intact shells, faint black and/or reddish mottling, and rare

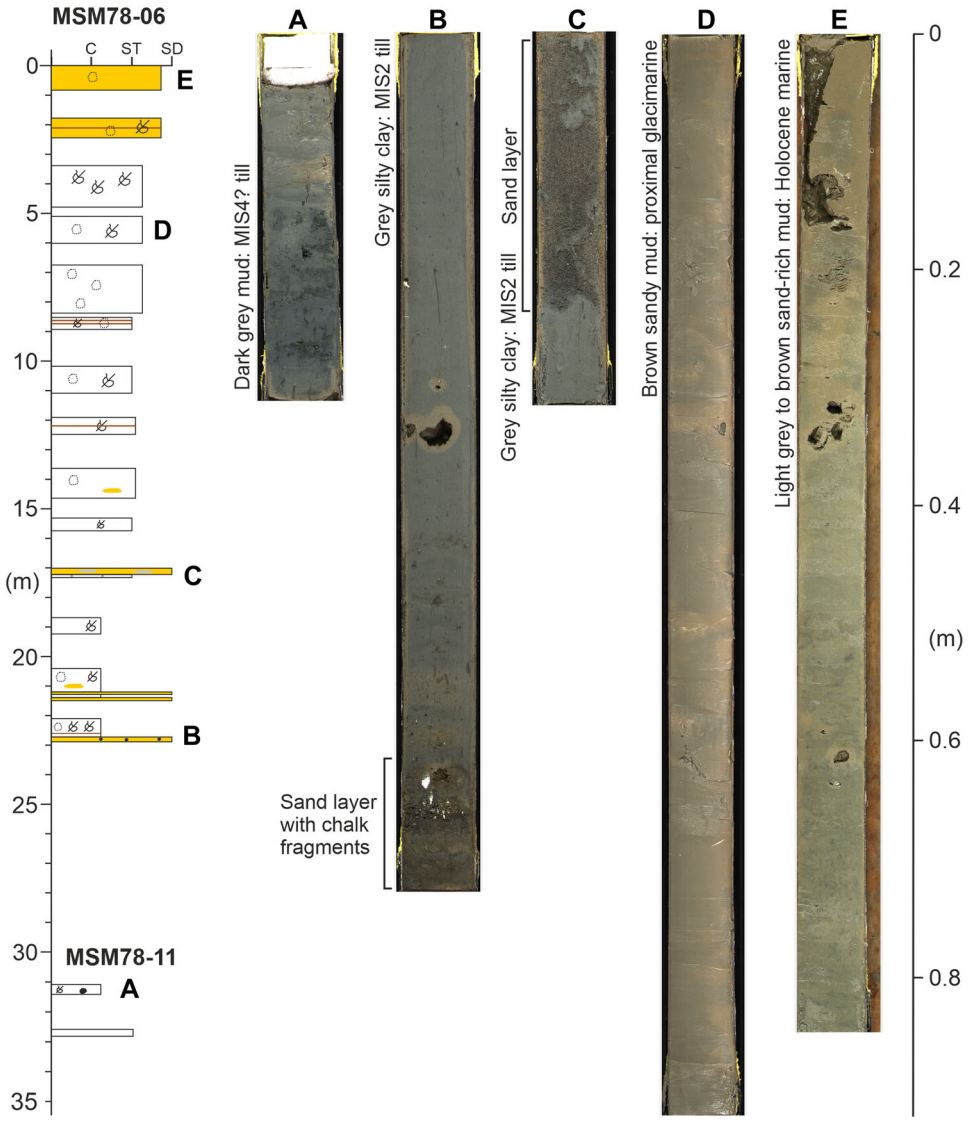

Figure 4. Selected core sections with corresponding lithological descriptions. (A) Dark grey till recovered in MSM78-11 (31–31.3 mbsf) corresponding to acoustic unit S3.2 of possible MIS4 age. (B) Grey till in MSM78-06 (22.1–22.83 mbsf) corresponding to acoustic unit S4.1 with sand layers containing chalk fragments eroded from west of the WGB and transported east by flow of the Witch Ground Ice Stream. (C) Sand layer overlying clay-rich stiff till in MSM78-06 (17–17.32 mbsf) corresponding to the upper part of acoustic unit S4.1 interpreted as evidence of hydraulic jacking at the ice–bed interface. Clayey material near the top right of the core section relates to coring disturbance. (D) Proximal glacimarine deposits in MSM78-06 (5.1–6.02 mbsf) corresponding to acoustic unit S5.1. (E) Sand-rich Holocene marine deposits from MSM78-06 (0–0.85 mbsf) corresponding to acoustic unit S5.2. [Color figure can be viewed at wileyonlinelibrary.com]

colour banding are also observed. From 2.5 mbsf to the seafloor (S5.2) consists of light grey to brown, sandy mud with black mottling, and occasional black laterally discontinuous colour banding with rare shell fragments (Fig. 4e).

Of the seven samples analysed for ^{14}C ages from MSM78-06 and MSM78-11, three returned usable ages, while the rest produced infinite ages >46 000 calendar age BP (cal a BP) (Table 1). The three ages correspond to 45 600 ± 2000 cal a BP at 32.78 mbsf (S3.2), 26 470 ± 170 cal year BP at 12.44 mbsf (bottom of S5.1) and 12 750 ± 70 cal year BP at 3.96 mbsf (top S5.1). Any geochronological method in glacial or formally glaciated environments is subject to reworking and contamination from ancient carbon, and thus we interpret these ages as maximum ages (Reinardy et al., 2018). Reworking and contamination probably also explain why five of the ages were infinite.

Interpretation and discussion

The two neighbouring coring sites of MSM78-11 and MSM78-06 recovered diamictons, which we interpret as subglacial to glacimarine in origin (not including the top 2.5 m of sediment cored in MSM78-06 which correspond to Holocene marine deposition) deposited below, or in proximity of the grounding of the Witch Ground Ice Stream (Fig. 3). We base this interpretation on multiple lines of evidence discussed in detail below but that broadly fit into four categories. First, the sedimentary character of these diamictons including distinct sand layers points to a subglacial or grounding line proximal depositional environment with occasional hydraulic jacking of ice from its bed (discussed in detail below). Second, the diamictons correspond to four acoustic units S3.2 to S5.1 (excluding marine deposits within S5.2) which along with characteristics such as chaotic and/or corrugated reflections can also be used to correlate the stratigraphy of MSM78-11 and MSM78-06 with neighbouring borehole sites that also recovered subglacial and glacimarine diamictons (Fig. 5). Third, seismic amplitude maps from the depth ranges of the described diamictons at MSM78-11 and MSM78-06 pick out at least five MSGL flowsets (Fig. 6). This provides a subglacial geomorphological context for the diamictons. Last, the chronological framework for MSM78-11

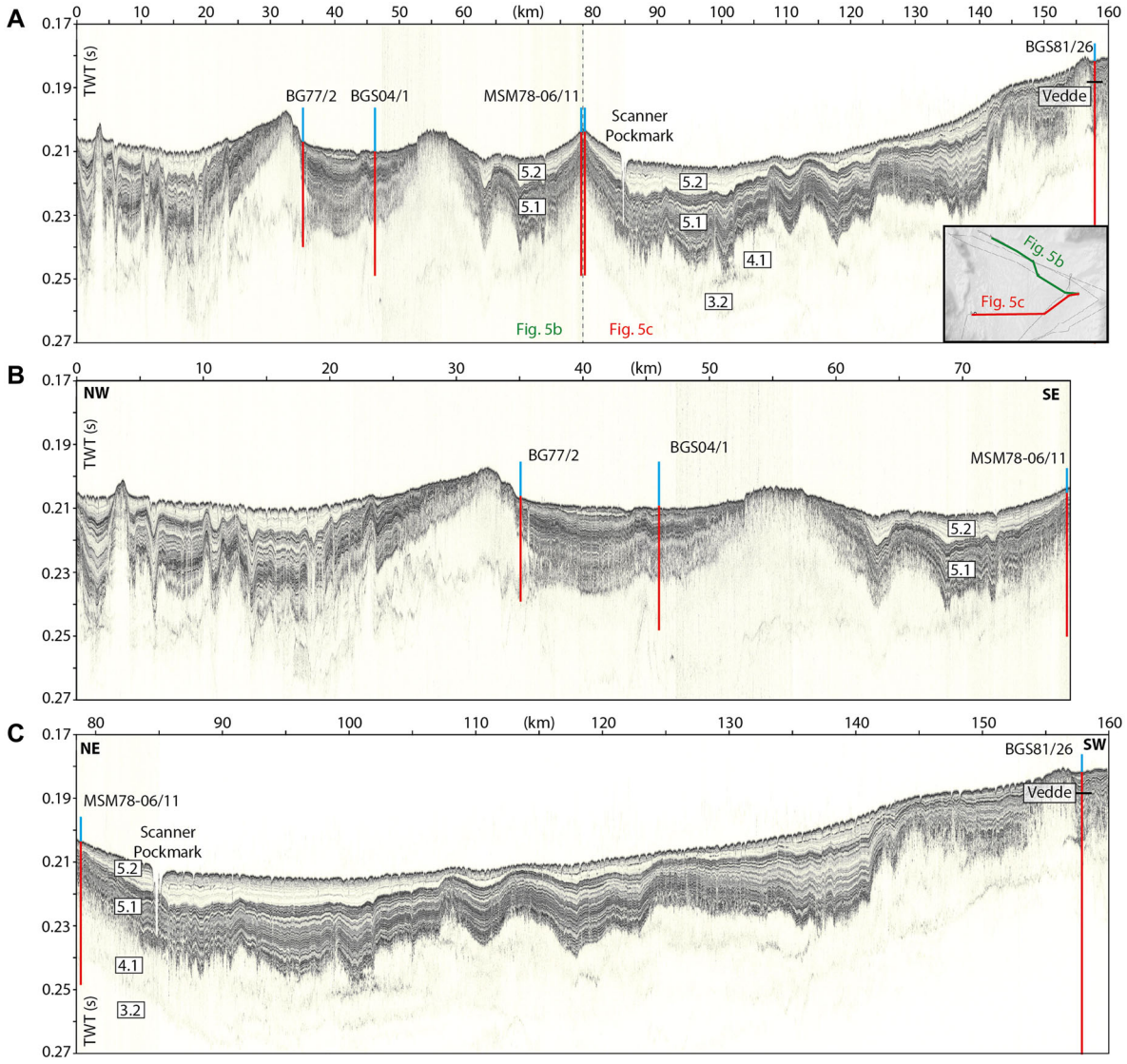

Figure 5. Correlation of the near-surface acoustic profile of MSM78-06 and MSM78-11 borehole sites (together labelled as MSM78-06/11 on profiles) with British Geological Survey borehole sites from across the WGB discussed in the text. Acoustic units S3.2–S5.2 are annotated on profiles in proximity to MSM78-06/11. Inset shows northern (green) and southern (red) profile locations that join at the eastern side of the WGB. Profile displayed in (A) is the entire northern and southern WGS profiles, profile (B) is the northern WGS profile and profile (C) is the southern WGS profile. Also included is the depth of the Vedde tephra (ash) horizon (12.1 ka) sampled in borehole BGS 81/26. Location of profiles within a regional context is shown in Fig. 1. [Color figure can be viewed at wileyonlinelibrary.com]

and MSM78-06 based on our own limited number of ^{14}C ages but also through correlation to well-dated neighbouring borehole sites indicates that the diamictons are associated with the most recent glaciation of the area during MIS2 and possibly MIS4.

Subglacial to glacimarine deposition in the WGB during MIS6 to MIS4

The upper Mid to Late Pleistocene sedimentary succession in the central northern North Sea consists of the Coal Pit, Swatchway and Witch Ground Formations (Stoker et al., 2011). The stratigraphically oldest sediments cored in this study come from MSM78-11 (34.17–33.72 mbsf) from the top of acoustic unit S3.2 that corresponds to the Coal Pit Formation (Figs. 2c, 3 and 5a). The Coal Pit Formation is interpreted as a glacimarine to subglacial deposit of MIS6 to MIS3 age (Davies et al., 2011). The consolidated, massive, sandy mud from MSM78-11 that includes shell fragments favours glacially overridden glacimarine or marine sediments rather than deposition in a glacimarine or marine environment (Fig. 4a). We interpret the shells as being reworked and incorporated into the mud during ice flow over glacimarine or marine sediments and broken up during shearing of the mud at the ice–bed interface. The low recovery of sediments at MSM78-11 meant that detailed structural analysis and further interpretation of the subglacial environment was limited. The sandy muds could correspond to a grounding line proximal glacimarine deposit or glacitectonite but considering the massive nature of the deposit along with the shell fragments, a subglacial traction till is more probable (*sensu* Evans et al., 2006). Our interpretation of a subglacial environment during deposition of these sediments also fits with the mapping of MSGL flowset 1 trending SW–NE (Figs. 6a and 7a) that may correspond to ice cover during MIS6-4. Flowset 1 is the stratigraphically deepest and oldest of the five flowsets mapped in this study. We interpret ice flow to the NE associated with MSGL flowset 1 because at no time during the Mid to Late Pleistocene do ice sheet models or empirical evidence suggest ice flow to the SW in our study area. Considering the orientation and stratigraphic position of

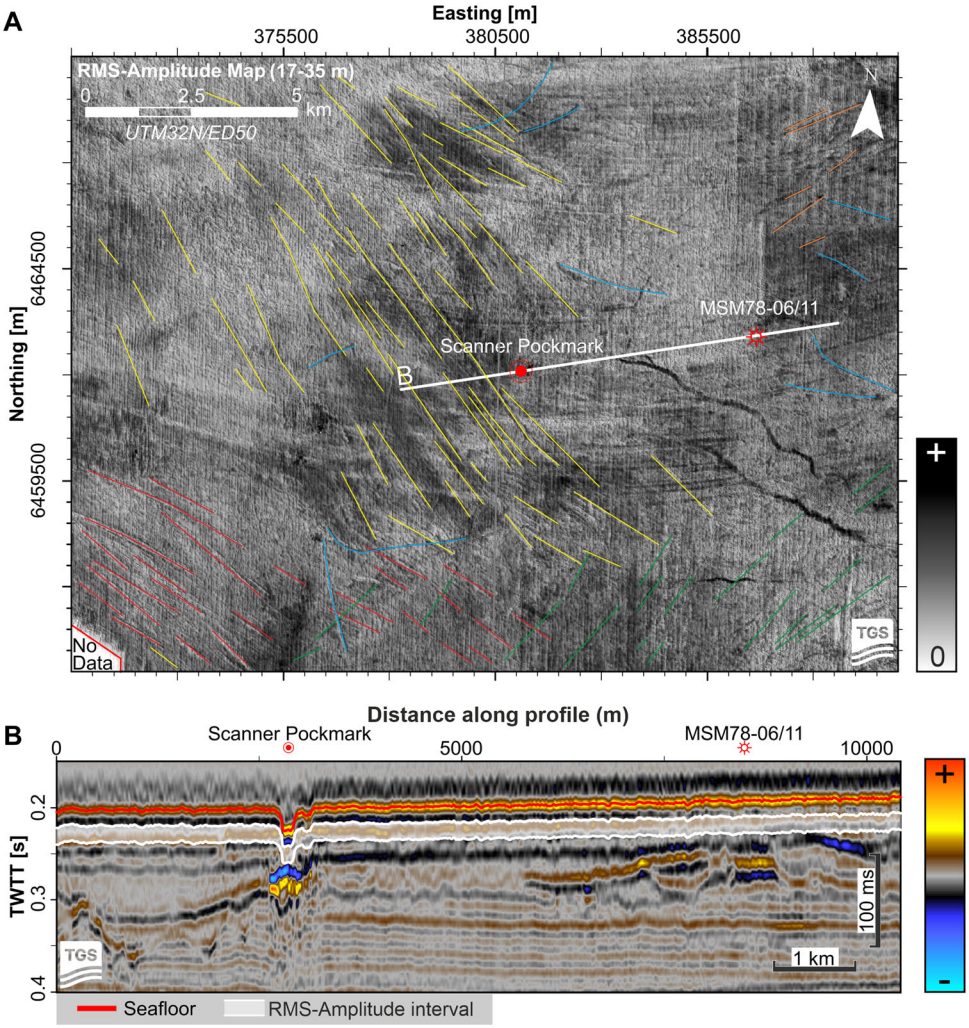

Figure 6. (A) Seismic root mean square (RMS) amplitude map at a depth interval between 17 and 35 mbsf produced from the CNS MegaSurvey. The orientations and interpreted ice flow direction corresponding to MSGL flowsets 1 (oldest) to 5 (youngest) are indicated. Blue lines indicate examples of iceberg scour. See Fig. 1 for location of map. White line is the location of seismic profile (B) while horizons marked in white in the profile indicate the amplitude interval used for the amplitude map. Corrugated horizons correspond to both MSGLs and iceberg scour marks at multiple stratigraphic depths including depths at which sediments were recovered at MSM-06/11. The seismic profile shows distance along the profile (m) on the *x*-axis and two-way travel time (s) on the *y*-axis. Source: seismic data courtesy of TGS. [Color figure can be viewed at wileyonlinelibrary.com]

MSGL flowset 1, it is possible that this flowset corresponds to MSGL flowset 2 of Graham et al. (2010). Based on our correlation of S3.2 in the echosounder data at the MSM78-11 coring site with regional mapping of subglacial features as well as chronological and stratigraphical constraints from neighbouring borehole sites in the WGB, we interpret these sediments as till deposited by the Witch Ground Ice Stream during MIS4 (Figs. 5 and 6). Our ^{14}C age of 45 600 ± 2000 cal BP at 33.78 mbsf at MSM78-11, while close to the oldest age range for ^{14}C, falls within the MIS4 age range, but we acknowledge that till deposited during MIS6 would probably give very similar results, i.e. ^{14}C ages close to infinite. If the till cored in MSM78-11 corresponds to deposition during MIS4, sedimentologically it is very similar to till deposited during MIS2 (Fig. 4a–c). To the south of the WGB, macroscopically similar till units were found to be microscopically distinct and were interpreted to represent grounded ice advances in MIS4 and MIS2 (Carr et al., 2000, 2006). The macroscopic similarity of the till may relate to both having been deposited by the Witch Ground Ice Stream (Fig. 7). We did not recover gravelly or sandy diamictons that have been reported from other parts of the North Sea that may correspond to grounded ice advance during MIS4 (Davies et al., 2011). Thus, we conclude that till deposited below the Witch Ground Ice Stream between MIS6 and MIS4 was relatively fine grained and massive. This probably relates to streaming ice overriding, deforming and homogenizing glacimarine sediments within the WGB (Fig. 7a).

Subglacial depositional processes and deposits of the Witch Ground Ice Stream during MIS2

Sediments recovered between 22.72 and 15.3 mbsf at MSM78-06 correspond to acoustic unit S4.1 and can be correlated to the Swatchway Formation (Figs. 2c and 3). They are sedimentologically similar to those recovered at MSM78-11 (silty clay) and are also interpreted as till (Fig. 4b, c). No usable ^{14}C ages were obtained from S4.1 sediments in MSM78-06 (Table 1), but it is possible to trace and correlate S4.1 from the MSM78-06 borehole site to BGS BH 04/01 and BGS 77/2 on echosounder profiles (Fig. 5a, b). The minimum age for corresponding tills at these sites is 32.4 ka (Sejrup et al., 2015) and 28.5 ka (Graham et al., 2010) at BGS BH 04/01 and 45.3 ka at 77/2 (Sejrup et al., 1994; 2015), the latter of which is probably reworked. Previously published amino acid geochronology at both 77/2 and BGS 81/26 (for which we also have direct correlation to MSM78-06 through the echosounder

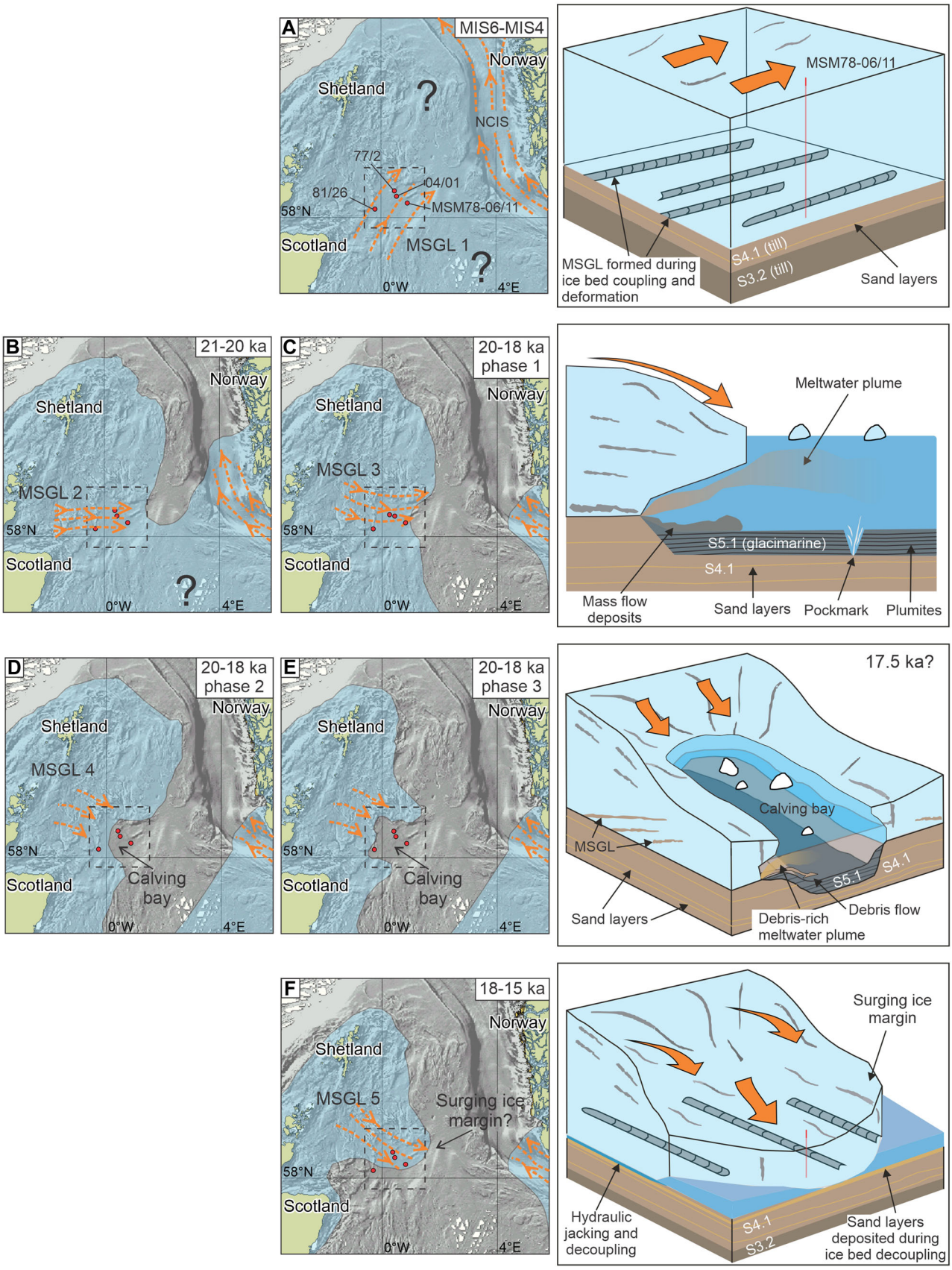

Figure 7. Ice flow history of the Witch Ground Ice Stream as interpreted from MSGL flowsets 1–5 outlined in Fig. 6(A). Streaming and possibly surging flow is linked to a depositional model that includes hydraulic jacking causing decoupling of the ice–bed interface and deposition of sand layers. As grounded ice retreated forming a calving bay within the WGB, glaciomarine deposition may have included mass flow deposits and plumites in a grounding line proximal setting. Areas within dashed black boxes have a depositional model depicted in the right-hand panels. NCIS = Norwegian Channel Ice Stream. Bathymetry is modified from Reinardy et al. (2018) and ice margins are based on interpretations by Batchelor et al. (2019), Bradwell et al. (2019), Evans et al. (2021) and Clark et al. (2022). [Color figure can be viewed at wileyonlinelibrary.com]

data) provides confirmation of a Late Pleistocene age (Fig. 5c) (Reinardy et al., 2018). In the echosounder data, S4.1 contains multiple discontinuous irregular internal reflections which correspond to MSGLs and iceberg scour marks that can be identified in seismic amplitude maps (Figs. 2c and 6). The corresponding diamictons in MSM78-06 contain distinct sand layers (Figs. 3 and 4b, c). We interpret this as both sedimentological and geomorphological evidence of streaming ice flow of the Witch Ground Ice Stream during the Late Pleistocene.

Apart from possibly MSGL flowset 1, we interpret MSGL flowsets 2–5 to correspond to the most recent ice cover in the area during MIS2 (Fig. 7b–f). We have interpreted ice flow direction associated with each MSGL flowset based on the evolving ice sheet configuration between 30 and 17 ka over the WGB as outlined by Gandy et al. (2021) and Clark et al. (2022). For flowsets 2–4 we have interpreted ice flow towards the east or southeast sourced from the BIIS since at no time during the last glacial cycle did the WGB receive ice flow from the east (Fig. 7b–d). In addition, chalk clasts within the diamicton recovered at MSM78-06 suggest ice flowing from approximately west or northwest across the WGB (Fig. 4b). The nearest source of chalk outcropping on the seafloor is to the west of the WGB (Andrews et al., 1990) which aligns with flowsets 2–4, and ice sourced over Scotland flowing east and southeast. After unzipping of the BIIS and FIS followed by marine water incursion into the WGB and formation of a calving bay around 20 ka, ice flow direction would have changed towards the east and southeast aligning with MSGL flowsets 3 and 4. The change from easterly (MSGL flowsets 2 and 3) to southeasterly ice flow (MSGL flowset 4) probably reflects the Witch Ground Ice Stream first sourced from the main BIIS to the west and then gradually more localized ice over Orkney and Shetland during overall deglaciation of the WGB as modelled by Clark et al. (2022) (Fig. 7b–e).

The orientation of MSGL flowset 5 could correspond to ice flow either to the northwest during maximum ice extent around 23–21 ka or alternatively to the southeast during ice sheet retreat between 21-17 ka. Because MSGL flowset 5 has a relatively shallow stratigraphic position, are relatively well preserved and cross-cut MSGL flowsets 2 and 3, we interpret MSGL flowset 5 to correspond to deglaciation of the WGB when ice flowed southeast sourced from a localized ice cap over Orkney and Shetland (Fig. 7f) (Bradwell et al., 2019). Localized readvances of ice at this time may be linked to the Fladen 1 and 2 events, dated to ~18–15 ka (Sejrup et al., 2015). It has also previously been suggested that these readvances may have corresponded to surging behaviour along the ice front and this would fit with our mapping of the distinct, cross-cutting MSGL flowset 5 (Figs. 6a and 7f). Thus, till recovered between 22.72 and 15.3 mbsf and corresponding to the upper part of S4.1 was probably deposited after the MIS2 maximum ice extent in the area during the final streaming event of the Witch Ground Ice Stream, possibly as part of surging behaviour along this sector of the ice margin (Fig. 7b–f).

The primarily massive nature of sediments cored from this interval (22.72–15.3 mbsf) probably corresponds to subglacially reworked glacimarine/marine sediments into a traction till leading to homogenization of the sediment at the bed of the Witch Ground Ice Stream (Fig. 4b). This interpretation comes with the same caveats as noted previously for traction till recovered in MSM78-11, i.e. a glacitectonite or grounding line proximal origin cannot be entirely dismissed. Our interpretation of a traction till contrasts with the corresponding diamicton recovered at BGS 04/01 25 km to the northwest of MSM78-06, which was comparatively coarser (higher concentrations of sand) and contained sheared and folded muds as well as flame structures interpreted as a glacitectonite (Graham et al., 2010; Sejrup et al., 2015). As noted for the older till below, the youngest till (MIS2) deposited by the Witch Ground Ice Stream is massive and finer grained compared to surrounding tills recovered at neighbouring borehole sites. Such compositional variations can affect the response of the till to changes in porewater pressure and/or any imposed shear stress as the concentrations of clay to sand influence hydraulic conductivity and hence the strength of coupling at the ice–bed interface (Kessler et al., 2013). Evidence of far more extreme temporal variations in porewater pressure at the ice–bed interface come in the form of the described sand layers between 22.72 and 17 mbsf within the till (Fig. 4b, c). These sand layers were probably deposited during the ice streaming event that formed MSGL flowsets 2–5 (Fig. 6a).

Ice–bed mechanical coupling is regulated by water pressure which in turn determines basal velocity (Weertman 1972; Alley et al., 1989; Kavanaugh and Clarke 2006; Damsgaard et al., 2020). The water pressure is affected by the type of subglacial drainage system, i.e. whether the system is distributed, consisting of a linked-cavity network, or channelized (Nye, 1970; Röthlisberger 1972; Walder and Fowler 1994). A cavity-dominated system is associated with high porewater pressure and promotes high basal velocities, while a channel-dominated system leads to comparatively lower porewater pressure and lower velocities (Damsgaard et al., 2016). Where cavities are hydraulically well connected to channels, they drain into efficient drainage systems, which tends to lower the overall basal water pressure and highlights the potential continuum between both systems (Chandler et al., 2013). At larger (>100 s m) scale, tunnel valleys in the North Sea Basin represent a channelized system (cf. Piotrowski 1997) but it is noticeable that in the WGB tunnel valleys primarily occur below S4.1. Indeed, Late Pleistocene age tunnel valleys exist below S4.1 directly to the NW and SW of the MSM78-11 and 06 borehole site (Fig. 6b) (Böttner et al., 2019; Callow et al., 2021). The distinct, well-sorted sand layers within the S4.1 till (22.72–17 mbsf) offer insights into the subglacial hydrology of the Witch Ground Ice Stream flowing across the WGB (Fig. 4b, c). We interpret the sand layers to represent decoupling of the ice stream from its bed due to rising porewater pressure (Figs. 3 and 6a–d). There are numerous examples of subglacial deposition of sorted sand layers by meltwater occurring during the uncoupling of the ice–bed interface (e.g. Piotrowski and Tulaczyk 1999; Piotrowski et al., 2006; Lesemann et al., 2010). Porewater pressure varies spatially and temporally across ice stream beds due to variations in the mechanical and hydraulic properties of underlying till as well as variations in meltwater supply (Damsgaard et al., 2016). This process forms a complex bed mosaic of 'sticky' spots or areas of the bed that deform and have strong coupling to the ice as well as areas where basal sliding is facilitated by (partial) decoupling of the ice–bed interface (Creyts and Schoof 2009; Phillips et al., 2018; Kasmalkar et al., 2021). Hydraulic jacking, where water films drain along the ice–bed interface, has been observed from modern ice streams and is sometimes accompanied by increases in ice flow velocity (Engelhardt and Kamb 1997; Doyle et al., 2022). Hydraulic jacking is particularly prevalent when the underlying till is clay-rich (Salamon 2014) as is the case in the WGB (Fig. 4c). This also explains the contrasting fine-grained nature of till deposited below the Witch Ground Ice Stream compared to sandier, coarser tills recovered from neighbouring borehole sites. The thicknesses of the sand layers in MSM78-06, which are minimum thickness measurements since some sand was probably washed out of the core barrel

during recovery, suggest water drained along the ice stream bed when the underlying porewater pressure in the subglacial traction till reached a critical level causing decoupling. From the evidence gathered here, these events were relatively rare, i.e. three to four decoupling events corresponding to four sand layers, but a greater number of sand layers may well exist in S4.1 considering no sediment was recovered below 22.72 mbsf plus wash out of the core barrel. There is also at least one additional example of massive sand layers within till of MIS2 age from the North Sea Basin (Ottesen et al., 2016). Borehole BH1004 is located in the southeastern North Sea on the Egersundbanken (Fig. 1). Similar to the WGB, two flowsets of MSGL (towards the NW and SSW) indicate ice streaming in the area possibly related to the neighbouring Norwegian Channel Ice Stream. Millimetre- to centimetre-scale sand layers are present within the till and may also relate to decoupling at the ice–bed interface.

Decoupling of the ice–bed interface would also be expected with surge behaviour of the BIIS margin in the vicinity of WGB (Fig. 7f). It is important to note that surging behaviour of marginal lobes has already been suggested for other sectors of the BIIS (Boston et al., 2010; Evans and Thomson 2010; Emery et al., 2019; Roberts et al., 2018b) and may have been the mechanism for the Fladen 1 and 2 readvances that probably extended across the WGB based on the prominent MSGL flowset 5 (Figs. 6a and 7f). At the least, readvances or ice margin oscillations are thought to be responsible for ice-marginal glacitectonics in the form of crevasse-squeeze ridges (also mapped as De Geer moraines) and areas of lobate composite moraine ridges (Graham et al., 2009; Evans et al., 2021) on the northern and northwestern margin of the WGS. These surges would have been accompanied by increases in basal water pressure, causing the ice to decouple from its bed (Piotrowski and Tulaczyk 1999; Kirkham et al., 2021). Decoupling and hydraulic jacking occur in distributed subglacial drainage systems which would appear to contrast with the hundreds of tunnel valleys that have been mapped across the North Sea Basin, indicating a channelized drainage system. However, both systems may have been present below the ice sheet in the North Sea as part of a continuum of the subglacial hydrological system. Indeed, there is evidence to suggests variable subglacial drainage systems between different ice sheets covering the North Sea Basin during the Mid to Late Pleistocene reflected in variable concentrations of corresponding tunnel valleys (e.g. Stewart and Lonergan, 2011). The bed of the palaeo-Norwegian Channel Ice Stream to the east is also notable for its lack of tunnel valleys and large (100 s m wide and 10 s km long) tunnel valleys have not been observed below modern ice streams (Kirkham et al., 2021, 2024). However, large drainage events have been observed below contemporary Antarctic ice streams that also influence ice flow velocity (Stearns et al., 2008; Siegfried et al., 2016). These drainage events are often sourced from subglacial lakes. Although evidence of subglacial lakes has not been found in the northern North Sea Basin, large proglacial lakes are thought to have existed during the LGM in the southern North Sea (Sejrup et al., 2016; Hjelstuen et al., 2018; Roberts et al., 2018b). However, we emphasize that subglacial lakes are not necessary for our interpretation of hydraulic jacking. The large number of tunnel valleys across the North Sea Basin demonstrate that large volumes of meltwater existed below the ice. Rapid drainage of supraglacial meltwater to the ice sheet bed through crevassing is commonly observed on the Greenland Ice Sheet and is a process suggested for tunnel valley inception in the North Sea Basin (Kirkham et al., 2021; 2024).

Proximal to distal glacimarine and marine deposits of the WGB during MIS2 to MIS1

The lower part of S5.1 (~15–13 mbsf), which corresponds to irregular, laterally discontinuous laminations, is interpreted to correspond to the transition from subglacial to grounding line proximal deposition (Figs. 2c and 5a–c). The corresponding sediments recovered in MSM78-06 are texturally similar to the subglacial sediments below in S4.1, but have slightly higher silt concentrations, appear lighter in colour as well as displaying colour banding and have rare occurrences of whole intact shells (Figs. 3 and 4d). Colour banding and intact shells would not be expected if these sediments were deformed and homogenized subglacially (i.e. as a traction till). Our grounding line proximal interpretation is also based on the acoustic character of S5.1 and using the echosounder data to correlate the lower part of S5.1 to neighbouring borehole BGS BH 04/01 (Fig. 5a, b). Recovered sediments include pebbles and/or dropstones and broken shell fragments within a sandy matrix at BGS BH 04/01 interpreted as a grounding line proximal deposit (Graham et al., 2010). This unit has been interpreted to mark the transition from subglacial to grounding line proximal deposition and has been dated to between 19.5 and 13.7 ka (Sejrup et al., 2015) and 16.2 and 11.9 ka (Graham et al., 2010) at BGS borehole BH 04/01 and dated between 26.6 and 17.7 ka in borehole BGS 77/2 (Fig. 5c) (Sejrup et al., 2015). The relatively large age range for these sediments at the different borehole sites probably reflects their grounding line proximal deposition where, similar to MSM78-06, reworking is very likely and indeed evidenced by associated debris flow deposits at BGS 77/2 (Fig. 7e) (Sejrup et al., 2015). The likelihood of grounding line oscillations and possible localized grounding line readvance (e.g. the Fladen 1 and 2 readvances) and/or scouring of these sediments by iceberg keels also explains possible reasons for such large age ranges. Indirect evidence of proximal grounding line deposition also comes from the analyses of gas migration pathways below the neighbouring Scanner pockmark. Callow et al. (2021) indicate gas accumulation on the boundary between S4.1 and S5.1. Modern and palaeo-grounding line proximal sediment deposits have been shown to have high permeability compared to more clay-rich distal glacimarine deposits and thus to be favourable for gas accumulation assuming an effective seal (e.g. Prothro et al., 2018; Ha et al., 2023).

It is uncertain whether the retreating ice front in the relatively deeper northern North Sea had a fringing ice shelf. Since the study area consists of a shallow basin, it is likely that during retreat of the grounding line, a calving bay may have formed (Fig. 7d, e). Observations from retreat of modern grounding lines suggest that the deepest areas of the bed along the ice front are the first to uncouple and float (Milillo et al., 2019; Schmidt et al. 2022). Rather than a distinct 'line' along the ice front, modern grounding lines operate within a grounding zone with cavities along the submarine ice front and tidal pumping causing cyclical coupling and uncoupling of the ice–bed interface within the grounding zone (Bamber et al., 2009; Rignot et al., 2011; Warburton et al., 2020; Freer et al., 2023). This type of grounding line proximal depositional environment, where reworking of sediment via mass flows (e.g. debris flows or turbidity currents) is likely, could explain why the acoustic characteristics of the lower part of S5.1 (~15–13 mbsf) contain disrupted or discontinuous laminations that more closely resembles the subglacial unit below (S4.1) (Fig. 2c). The interpretation of a calving bay in the WGB aligns with previous deglaciation patterns for this part of the central North Sea (Sejrup et al., 1987; Bradwell et al., 2008; Graham et al., 2010; Merritt et al., 2017; Clark et al., 2022).

The acoustically well-laminated mid and upper part of S5.1 (~13–2.5 mbsf) corresponds to the Witch Ground Formation and probably more distal grounding line deposition in comparison to the disrupted laminations of the lower part of S5.1 (Fig. 2c). However, considering the likely high deposition rates for S5.1 discussed below, grounded ice may still have been locally present, i.e. along the margins of the WGB. A radiocarbon age of 12 750 ± 70 cal a BP was obtained at the top of S5.1 (3.96 mbsf), while the age of 26 470 ± 170 cal a BP obtained towards the base of S5.1 (12.44 mbsf) is probably too old due to reworking or contamination (Table 1). Previous studies have demonstrated that glacimarine conditions persisted in the central North Sea until after 12 ka based on the ages of iceberg-scoured horizons (Stoker & Long 1984; Graham et al., 2010). The well-laminated acoustic appearance of S5.1 in echosounder data is common in glacimarine environments dominated by deposition from meltwater plumes, i.e. plumites (e.g. O'Regan et al., 2021). These sediments must have been deposited after grounded ice retreat from the WGS after ~15 ka and before ~12 ka possibly directly after the Fladen 1 and 2 readvances (defined by the mapped Fladen 1 and 2 moraines) with the grounding line retreating to the vicinity of the northern margin of the WGS. This interpretation is consistent with the well-defined, high-reflectance and laterally continuous laminated character of S5.1 (Fig. 5).

Another distinct characteristic of ice-proximal glacimarine environments are high deposition rates compared to marine deposition rates. At the MSM78-06 borehole site, in contrast to the relatively thin layer of overlying marine Holocene age sediments (S5.2), the thick nature of S5.1 (~11.26 m in MSM78-06) along with the radiocarbon age of 12.7 ka at the top suggests deposition rates possibly as high ~260 cm ka^{-1} assuming ice retreat and transition from subglacial to glacimarine deposition took place around 17 ka (Sejrup et al., 2016). This is a broad estimate and deposition rates are rarely constant in glacimarine environments and can range from 1 to 24 mm a^{-1} in modern glacimarine environments, largely reflecting proximity to the grounding line, sediment supply and variable glacier dynamics (e.g. Boldt et al., 2013). Even considering the ^{14}C age obtained from the base of MSM78-06 of 26 470 ± 170 cal a BP, which is probably too old and reworked, the deposition rate of S5.1 would be 80 cm ka^{-1}. This rate is considerably higher than modern-day deposition rates (de Haas et al., 1996), but is similar to rates calculated for the mid Pleistocene, which also coincided with glacimarine conditions in the northern North Sea (Reinardy et al., 2017).

The top 2.5 m of MSM78-06 correspond to S5.2 and the marine upper Witch Ground Formation of Holocene age (Figs. 2c and 4e). This age is confirmed by correlation via echosounder data to BGS 81/26 that contains the Vedde ash (12.1 ka) at the approximate transition from distal glacimarine to marine deposition (Fig. 5c) (Sejrup et al., 1987). This is reflected in the sandy mud of the upper 2.5 m of MSM78-06 and a significantly reduced deposition rate compared to S5.1. Sandy muds probably correspond to increasing current-influenced sedimentation possibly including winnowing of fines. Increasing sand content and decreasing deposition rate within Holocene sediments in the North Sea has been reported by previous studies (Erlenkeuser, 1979; Johnson & Elkins, 1979; Lehman & Keigwin 1992; de Haas et al., 1996).

The Witch Ground Ice Stream in a local and regional context

Both the BIIS and FIS are well constrained and dated through the most recent glacial cycle, i.e. from location, timing and glaciological dynamics of maximum ice sheet extent and proceeding retreat (including readvances) all of which varied from sector to sector (Clark et al., 2022). The Witch Ground Ice Stream was probably an important glaciological feature not only of ice cover in the North Sea but also in governing the overall dynamics of the BIIS. The limited chronology from MSM78-06 is not able to distinguish if the Witch Ground Ice Stream was present during ice sheet build up and maximum extent or if it related primarily to driving deglaciation of the North Sea. However, the preservation of multiple sets of variably orientated MSGLs suggests changing ice flow direction over a relatively short (<1 glacial cycle) period of time. This fits with the complex modelled migration of ice divides over the WGB during maximum ice extent and subsequent retreat between 24 and 18 ka (Clark et al., 2022). During this time the main North Sea ice divide moved north across the WGB while a smaller ice divide linked to ice accumulation over Orkney and Shetland migrated east across the WGB. Streaming would not occur in the WGB when covered by an ice divide but the migration of ice divides across the WGB would have changed the regional ice sheet geometry and the Witch Ground Ice Stream and its changing flow direction may well be a consequence of this rapidly changing ice sheet geometry. What has also been suggested is that once unzipping and rapid deglaciation occurred across the North Sea, the northern North Sea may have seen a complex final phase of localized deglaciation with multiple independent ice caps or ice domes situated to the north and northwest of the WGB over Shetland and Pobie Bank, and to the south over Dogger Bank (Fig. 1) (Evans et al., 2021; Gandy et al., 2021; Clark et al., 2022). Both sedimentological evidence (chalk clasts) and geomorphological evidence (MSGL flowsets) seem to support this assertion.

Both model and empirical data indicate that deglaciation of the entire BIIS was initiated by retreat of the Norwegian Channel Ice Stream causing the unzipping from the FIS which then led to rapid deglaciation or collapse of the ice sheet across the North Sea (Gandy et al., 2021). The Witch Ground Ice Stream is key in this rapid deglaciation. Modelling by Clark et al. (2022) indicate that at 20 ka directly after unzipping, a calving bay forms in the vicinity of the WGB which is topographically lower (>140 m water depth) than the surrounding North Sea (Fig. 7d, e). At this point, the largest area of streaming ice around the entire BIIS is found along the ice margin covering the WGB (Clark et al., 2022). This probably corresponds to an active period of the Witch Ground Ice Stream that was drawing down considerable volumes of ice from the entire North Sea sector of the BIIS. This modelled streaming event corresponds with MSGL flowsets 2–4 and till sequences discussed in this study (Fig. 7b–e). Rapid retreat of the grounding line in the North Sea is thought to have been driven by a calving-induced ice stream–elevation line altitude (ELA) feedback (Clark et al., 2022). This suggests that as the grounding line of the Witch Ground Ice Stream reached the deeper waters around the WGB, calving flux would have increased producing upstream thinning of the ice stream surface, lowering elevations below the ELA and increasing surface melting, sufficient to trigger widespread rapid ice-sheet retreat from areas of deep water (Clark et al., 2022). Increased surface melting and large volumes of meltwater would also explain the relatively thick grounding line proximal glacimarine deposits (S5.1) described in this study (Fig. 2c).

As noted previously, there are several well-defined and dated ice stream landsystems from around both the BIIS and the FIS. Here we make some brief observations regarding similarities and differences to the Witch Ground Ice Stream. First, unlike the Norwegian Channel Ice Stream to the east and the North Sea Lobe ice stream to the west, there is no clear

onset zone, lateral (shear) boundaries or calving margin for the Witch Ground Ice Stream and thus we do not see a mixed-bed geomorphological imprint (e.g. Roberts et al., 2018b) but rather an imprint dominated by MSGLs. Both the aforementioned ice streams also have prominent grounding zone wedges along their bed while these features are lacking from the Witch Ground Ice Stream bed although recessional moraines have been mapped to the west and northwest of the WGB (Evans et al., 2021). This is to be expected considering the rapid deglaciation discussed above which would not have favoured stabilization of the grounding line and deposition of grounding zone wedges. In addition, a relatively flat and soft bed lacking rock outcrops and pinning points would also limit prolonged grounding line stability but rather provide ample subglacial sediment to be eroded, advected and/or deformed into MSGLs. A significant challenge for Clark et al. (2022) was aligning their model reconstruction of the BIIS with some of the empirically defined ice stream limits. They suggest that one possibility is that their model does not consider subglacial water or drainage instabilities that might be required to produce a non-steady oscillation or surge of the ice margin. This study presents the first empirical evidence of such a subglacial water instability causing hydraulic jacking.

Conclusion

Analyses of sediments deposited at the bed of the Witch Ground Ice Stream indicate that sorted sand layers within massive diamicton are typical and distinct from other descriptions of tills from the North Sea Basin. The sand layers are interpreted to correspond to subglacial deposition during hydraulic jacking at the ice–bed interface of the Witch Ground Ice Stream during multiple streaming events. In contrast to previous studies that have described glacitectonites deposited below the most recent grounded ice in the WGB, we only recovered massive diamictons that did not contain any obvious deformation structures. This in turn suggests deposition of a subglacial traction till with a relatively strong ice–bed coupling, but regular increases of porewater pressure, partially made possible by the clay-rich sediments below, would have allowed decoupling at the bed. Hydraulic jacking and decoupling at the ice–bed interface was probably at least partially responsible for streaming and possibly surging ice flow of the Witch Ground Ice Stream across the WGB and corresponds to the multiple MSGL flowsets. The oldest MSGL flowset 1 may correspond to the northeast flow of the Witch Ground Ice Stream during MIS6-4. Based on chalk clasts within the subglacial traction till we link MSGL flowsets 2–4 to east and southeast flow of the Witch Ground Ice Stream as the BIIS retreated towards the Scottish coast. In the final stage of deglaciation, ice readvance to the southeast possibly through surging and sourced from a localized ice cap over Shetland and Orkney may correspond to the Fladen 1 and/or 2 ice readvance and formation of MSGL flowset 5. The transition from subglacial to glacimarine deposition is well defined in acoustic records, but the corresponding sediments are surprisingly uniform apart from a distinct change in colour from grey (subglacial) to brown occasionally colour banded stiff mud with silt and sand lenses and intact shells (glacimarine). High deposition rates (260–80 cm ka^{-1}) during grounding line proximal to distal deposition may also correspond to plumites reflected in the well-defined laminations apparent in acoustic records of the glacimarine sediments.

Acknowledgements. This work received funding from the European Union's Horizon 2020 research and innovation programme under grant agreement No. 654462 (STEMM-CCS) and the Natural Environment Research Council (CHIMNEY; NERC Highlight Topic; NE/N016130/1). We would like to thank all those involved in the planning and acquisition of data during research cruise MSM78, including the officers, engineers and crews, the scientific parties, and all seagoing technicians and engineers. The British Ocean Sediment Core Research Facility (BOSCORF) is thanked for the use of their facilities. We acknowledge TGS for access to the CNS MegaSurvey. Lastly, we would like to thank an anonymous reviewer alongside a particularly insightful review from Andy Emery that helped greatly improve the original text.

Data Availability Statement

The data that support the findings of this study are available from the corresponding author upon reasonable request.

Abbreviations. AMS, Accelerator Mass Spectrometry; BGS, British Geological Survey; BIIS, British and Irish Ice Sheet; cal a BP, Calendar age; *cf.*, *Confer*; FIS, Fennoscandian Ice Sheet; *sensu*, *In the sense of*; LARS, Launch and Recovery System; LGM, Last Glacial Maximum; MIS, Marine Isotope Stage; MSGLs, Mega-scale glacial lineations; mbsf, Metres below seafloor; NCIS, Norwegian Channel Ice Stream; RMS, Root Mean Square; SBP, Subbottom profiler; TWT, Two-way travel time; WGB, Witch Ground Basin.

References

Alley, R.B., Blankenship, D.D., Rooney, S.T. & Bentley, C.R. (1989) Water-pressure coupling of sliding and bed deformation: III. Application to Ice Stream-B, Antarctica. *Journal of Glaciology*, 35, 130–139.

Andrews, I., Long, D., Richards, P., Thomson, A., Brown, S. & Chesher, J. et al. (1990) *The geology of the moray firth: memoir of the British Geological Survey*. HMSO: London.

Bamber, J.L., Gomez-Dans, J.L. & Griggs, J.A. (2009) A new 1 km digital elevation model of the Antarctic derived from combined satellite radar and laser data—Part 1: Data and methods. *The Cryosphere*, 3, 101–111.

Batchelor, C.L., Margold, M., Krapp, M., Murton, D.K., Dalton, A.S., Gibbard, P.L. et al. (2019) The configuration of Northern Hemisphere ice sheets through the Quaternary. *Nature Communications*, 10, 3713.

Boldt, K.V., Nittrouer, C.A., Hallet, B., Koppes, M.N., Forrest, B.K., Wellner, J.S. et al. (2013) Modern rates of glacial sediment accumulation along a 15°S-N transect in fjords from the Antarctic Peninsula to southern Chile. *Journal of Geophysical Research: Earth Surface*, 118, 2072–2088.

Boston, C.M., Evans, D.J.A. & Cofaigh, C.Ó. (2010) Styles of till deposition at the margin of the last glacial maximum North Sea lobe of the British–Irish ice sheet: an assessment based on geochemical properties of glacigenic deposits in Eastern England. *Quaternary Science Reviews*, 29, 3184–3211.

Böttner, C., Berndt, C., Reinardy, B.T.I., Geersen, J., Karstens, J., Bull, J.M. et al. (2019) Pockmarks in the Witch Ground Basin, central North Sea. *Geochemistry, Geophysics, Geosystems*, 20, 1698–1719.

Bradwell, T., Small, D., Fabel, D., Clark, C.D., Chiverrell, R.C., Saher, M.H. et al. (2019) Pattern, style and timing of British-Irish Ice Sheet retreat: Shetland and northern North Sea sector. *Journal of Quaternary Science*, 36, 681–722.

Bradwell, T., Stoker, M.S., Golledge, N.R., Wilson, C.K., Merritt, J.W., Long, D. et al. (2008) The northern sector of the last British Ice Sheet: Maximum extent and demise. *Earth-Science Reviews*, 88, 207–226.

Buckley, F.A. (2017) A glaciogenic sequence from the Early Pleistocene of the Central North Sea. *Journal of Quaternary Science*, 32, 145–168.

Callard, S.L., Ó Cofaigh, C., Benetti, S., Chiverrell, R.C., Van Landeghem, K.J.J., Saher, M.H. et al. (2020) Oscillating retreat of the last British-Irish Ice Sheet on the continental shelf offshore Galway Bay, western Ireland. *Marine Geology*, 420, 106087.

Callow, B., Bull, J.M., Provenzano, G., Böttner, C., Birinci, H., Robinson, A.H. et al. (2021) Seismic chimney characterisation in the North Sea – Implications for pockmark formation and shallow gas migration. *Marine and Petroleum Geology*, 133, 105301.

Carr, S.J., Haflidason, H. & Sejrup, H.P. (2000) Micromorphological evidence supporting Late Weichselian glaciation of the Northern North Sea. *Boreas*, 29, 315–328.

Carr, S.J., Holmes, R., van der Meer, J.J.M. & Rose, J. (2006) The last glacial maximum in the North Sea basin: micromorphological evidence of extensive glaciation. *Journal of Quaternary Science*, 21, 131–153.

Chandler, D.M., Wadham, J.L., Lis, G.P., Cowton, T., Sole, A., Bartholomew, I. et al. (2013) Evolution of the subglacial drainage system beneath the Greenland Ice Sheet revealed by tracers. *Nature Geoscience*, 6, 195–198.

Clark, C.D., Ely, J.C., Hindmarsh, R.C.A., Bradley, S., Ignéczi, A., Fabel, D. et al. (2022) Growth and retreat of the last British–Irish Ice Sheet, 31 000 to 15 000 years ago: the BRITICE-CHRONO reconstruction. *Boreas*, 51, 699–758.

Creyts, T.T. & Schoof, C.G. (2009) Drainage through subglacial water sheets. *Journal of Geophysical Research: Earth Surface*, 114. Available at: https://doi.org/10.1029/2008JF001215

Damsgaard, A., Egholm, D.L., Beem, L.H., Tulaczyk, S., Larsen, N.K., Piotrowski, J.A. et al. (2016) Ice flow dynamics forced by water pressure variations in subglacial granular beds. *Geophysical Research Letters*, 43, 12,165–12,173.

Damsgaard, A., Goren, L. & Suckale, J. (2020) Water pressure fluctuations control variability in sediment flux and slip dynamics beneath glaciers and ice streams. *Communications Earth & Environment*, 1, 66.

Davies, B.J., Roberts, D.H., Bridgland, D.R., Cofaigh, C.Ó. & Riding, J.B. (2011) Provenance and depositional environments of Quaternary sediments from the western North Sea basin. *Journal of Quaternary Science*, 26, 59–75.

de Haas, H., Okkels, E. & van Weering, T.C.E. (1996) Recent sediment accumulation in the Norwegian Channel, North Sea. *Norwegian geologiske undersøkelse Bulletin*, 430, 57–65.

Dove, D., Evans, D.J.A., Lee, J.R., Roberts, D.H., Tappin, D.R., Mellett, C.L. et al. (2017) Phased occupation and retreat of the last British-Irish Ice Sheet in the southern North Sea: geomorphic and seismostratigraphic evidence of a dynamic ice lobe. *Quaternary Science Reviews*, 163, 114–134.

Doyle, S.H., Hubbard, B., Christoffersen, P., Law, R., Hewitt, D.R., Neufeld, J.A. et al. (2022) Water flow through sediments and at the ice-sediment interface beneath Sermeq Kujalleq (Store Glacier), Greenland. *Journal of Glaciology*, 68, 665–684.

Emery, A.R., Hodgson, D.M., Barlow, N.L.M., Carrivick, J.L., Cotterill, C.J. & Phillips, E. (2019) Left High and Dry: Deglaciation of Dogger Bank, North Sea, Recorded in Proglacial Lake Evolution. *Frontiers in Earth Science*, 7, 1–27.

Engelhardt, H. & Kamb, B. (1997) Basal hydraulic system of a West Antarctic ice stream: Constraints from borehole observations. *Journal of Glaciology*, 43, 207–230.

Erlenkeuser, H. (1979) Environmental effects on radiocarbon in coastal marine sediments. In: Berger, R. & Suess, H., (eds) *Radiocarbon dating*. Berkeley: University of California Press. pp. 453–469.

Evans, D.J.A., Phillips, E.R., Hiemstra, J.F. & Auton, C.A. (2006) Subglacial till: Formation, sedimentary characteristics and classification. *Earth-Science Reviews*, 78, 115–176.

Evans, D.J.A., Roberts, D.H., Bateman, M.D., Clark, C.D., Medialdea, A., Callard, L. et al. (2021) Retreat dynamics of the eastern sector of the British–Irish Ice Sheet during the last glaciation. *Journal of Quaternary Science*, 36, 723–751.

Evans, D.J.A. & Thomson, S.A. (2010) Glacial sediments and landforms of Holderness, eastern England: a glacial depositional model for the North Sea Lobe of the British–Irish Ice Sheet. *Earth-Science Reviews*, 101, 147–189.

Freer, B.I.D., Marsh, O.J., Hogg, A.E., Fricker, H.A. & Padman, L. (2023) Modes of Antarctic tidal grounding line migration revealed by Ice, Cloud, and land Elevation Satellite-2 (ICESat-2) laser altimetry. *The Cryosphere*, 17, 4079–4101.

Funder, S., Sørensen, A.H.L., Larsen, N.K., Bjørk, A.A., Briner, J.P., Olsen, J. et al. (2021) Younger Dryas ice margin retreat in Greenland: new evidence from southwestern Greenland. *Climate of the Past*, 17, 587–601.

Gafeira, J., Dolan, M.F.J. & Monteys, X. (2018) Geomorphometric characterization of pockmarks by using a GIS-based semi-automated toolbox. *Geosciences*, 8, 154.

Gandy, N., Gregoire, L.J., Ely, J.C., Clark, C.D., Hodgson, D.M., Lee, V. et al. (2018) Marine ice sheet instability and ice shelf buttressing of the Minch Ice Stream, northwest Scotland. *The Cryosphere*, 12, 3635–3651.

Gandy, N., Gregoire, L.J., Ely, J.C., Cornford, S.L., Clark, C.D. & Hodgson, D.M. (2021) Collapse of the last Eurasian Ice Sheet in the North Sea modulated by combined processes of ice flow, surface melt, and marine ice sheet instabilities. *Journal of Geophysical Research: Earth Surface*, 126, e2020JF005755.

Goslar, T. (2015) *Description of procedures of AMS 14 C dating used in the Poznań Radiocarbon Laboratory*. https://radiocarbon.pl/en/description_of-procedures/

Graham, A., Lonergan, L. & Stoker, M. (2007) Evidence for Late Pleistocene ice stream activity in the Witch Ground Basin, central North Sea, from 3D seismic reflection data. *Quaternary Science Reviews*, 26, 627–643.

Graham, A.G.C., Lonergan, L. & Stoker, M.S. (2009) Seafloor glacial features reveal the extent and decay of the last British Ice Sheet, east of Scotland. *Journal of Quaternary Science*, 24, 117–138.

Graham, A.G.C., Lonergan, L. & Stoker, M.S. (2010) Depositional environments and chronology of Late Weichselian glaciation and deglaciation in the central North Sea. *Boreas*, 39, 471–491.

Graham, A.G.C., Stoker, M.S., Lonergan, L. et al. (2011) The Pleistocene glaciations of the North Sea basin. In: Ehlers, J., Gibbard, P.L., Hughes, P.D. (Eds) *Developments in Quaternary Science: Quaternary Glaciations–Extent and Chronology: a Closer Look*. Elsevier: Amsterdam. pp. 261–268.

Ha, S., Lee, J.I., Bak, Y.S., Yoo, K.C. & Khim, B.K. (2023) Paleoenvironmental reconstruction of glaciomarine sediments in the Drygalski Basin of the western Ross Sea since the Last Glacial Maximum. *Sedimentary Geology*, 456, 106495.

Haavik, K.E. & Landrø, M. (2014) Iceberg ploughmarks illuminated by shallow gas in the central North Sea. *Quaternary Science Reviews*, 103, 34–50.

Heaton, T.J., Köhler, P., Butzin, M., Bard, E., Reimer, R.W., Austin, W.E.N. et al. (2020) MARINE20–the marine radiocarbon age calibration curve (0-55,000 CAL BP). *Radiocarbon*, 62, 779–820.

Hjelstuen, B.O., Sejrup, H.P., Valvik, E. & Becker, L.W.M. (2018) Evidence of an ice dammed lake outburst in the North Sea during the last deglaciation. *Marine Geology*, 402, 118–130.

Hughes, A.L.C., Gyllencreutz, R., Lohne, Ø.S., Mangerud, J. & Svendsen, J.I. (2016) The last Eurasian ice sheets–a chronological database and time-slice reconstruction, DATED-1. *Boreas*, 45, 1–45.

Johnson, T.C. & Elkins, S.R. (1979) Holocene deposits of the northern North Sea evidence for dynamic control of their mineral and chemical composition. *Geologie en Mijnbouw*, 58, 353–366.

Judd, A., Long, D. & Sankey, M. (1994) Pockmark formation and activity, UK block 15/25, North Sea. *Bulletin of the Geological Society of Denmark*, 41, 34–49.

Kasmalkar, I., Damsgaard, A., Goren, L. et al. (2021) Shear variation at the ice-till interface changes the spatial distribution of till porosity and meltwater drainage. *Journal of Geophysical Research: Earth Surface*, 126, e2021JF006460. Available at: https://doi.org/10.1029/2021JF006460

Kavanaugh, J.L. & Clarke, G.K.C. (2006) Discrimination of the flow law for subglacial sediment using in situ measurements and an interpretation model. *Journal of Geophysical Research: Earth Surface*, 111. Available at: https://doi.org/10.1029/2005JF000346

Kessler, T.C., Comunian, A., Oriani, F., Renard, P., Nilsson, B., Klint, K.E. et al. (2013) Modeling Fine-Scale Geological Heterogeneity—Examples of Sand Lenses in Tills. *Groundwater*, 51, 692–705.

Kirkham, J.D., Hogan, K.A., Larter, R.D., Arnold, N.S., Ely, J.C., Clark, C.D. et al. (2024) Tunnel valley formation beneath deglaciating mid-latitude ice sheets: Observations and modelling. *Quaternary Science Reviews*, 323, 107680.

Kirkham, J.D., Hogan, K.A., Larter, R.D., Self, E., Games, K., Huuse, M. et al. (2021) Tunnel valley infill and genesis revealed by high-resolution 3-D seismic data. *Geology*, 49, 1516–1520.

Lehman, S.J. & Keigwin, L.D. (1992) Sudden changes in North Atlantic circulation during the last deglaciation. *Nature*, 356, 757–762.
Lesemann, J.E., Alsop, G.I. & Piotrowski, J.A. (2010) Incremental subglacial meltwater sediment deposition and deformation associated with repeated ice-bed decoupling: a case study from the Island of Funen, Denmark. *Quaternary Science Reviews*, 29, 3212–3229.
Merritt, J.W., Connell, E.R. & Hall, A.M. (2017) Middle to Late Devensian glaciation of north-east Scotland: implications for the north-eastern quadrant of the last British–Irish ice sheet. *Journal of Quaternary Science*, 32, 276–294.
Milillo, P., Rignot, E., Rizzoli, P., Scheuchl, B., Mouginot, J., Bueso-Bello, J. et al. (2019) Heterogeneous retreat and ice melt of Thwaites Glacier, West Antarctica. *Science Advances*, 5, eaau3433.
Morén, B.M., Sejrup, H.P., Hjelstuen, B.O., Borge, M.V. & Schäuble, C. (2017) The last deglaciation of the Norwegian Channel – geomorphology, stratigraphy and radiocarbon dating. *Boreas*, 47, 347–366.
Newton, A.M.W., Montelli, A., Batchelor, C.L., Bellwald, B., Harding, R., Huuse, M. et al. (2024) Glacial seismic geomorphology and Plio-Pleistocene ice sheet history offshore NW Europe. *Geological Society, London, Special Publications*, 525, 111–140. Available at: https://doi.org/10.1144/SP525-2023-117
Nye, J.F. (1970) Glacier sliding without cavitation in a linear viscous approximation. *Proceeding of the Royal Society of London Series A*, 315, 381–403.
O'Regan, M., Cronin, T.M., Reilly, B., Alstrup, A.K.O., Gemery, L., Golub, A. et al. (2021) The Holocene dynamics of Ryder Glacier and ice tongue in north Greenland. *The Cryosphere*, 15, 4073–4097.
Ottesen, D., Batchelor, C.L., Dowdeswell, J.A. & Løseth, H. (2018) Morphology and Pattern of Quaternary Sedimentation in the North Sea Basin (52-62°N). *Marine and Petroleum Geology*, 98, 836–859.
Ottesen, D., Dowdeswell, J.A. & Bugge, T. (2014) Morphology, sedimentary infill and depositional environments of the Early Quaternary North Sea Basin (56-62°N). *Marine and Petroleum Geology*, 56, 123–146.
Ottesen, D., Stokes, C.R., Bøe, R., Rise, L., Longva, O., Thorsnes, T. et al. (2016) Landform assemblages and sedimentary processes along the Norwegian Channel Ice Stream. *Sedimentary Geology*, 338, 115–137.
Patton, H., Hubbard, A., Andreassen, K., Auriac, A., Whitehouse, P.L., Stroeven, A.P. et al. (2017) Deglaciation of the Eurasian ice sheet complex. *Quaternary Science Reviews*, 169, 148–172.
Patton, H., Hubbard, A., Andreassen, K., Winsborrow, M. & Stroeven, A.P. (2016) The build-up, configuration, and dynamical sensitivity of the Eurasian ice-sheet complex to Late Weichselian climatic and oceanic forcing. *Quaternary Science Reviews*, 153, 97–121.
Phillips, E., Spagnolo, M., Pilmer, A.C.J., Rea, B.R., Piotrowski, J.A., Ely, J.C. et al. (2018) Progressive ductile shearing during till accretion within the deforming bed of a palaeo-ice stream. *Quaternary Science Reviews*, 193, 1–23.
Piotrowski, J.A. (1997) Subglacial hydrology in northwestern Germany during the last glaciation: groundwater flow, tunnel valleys and hydrological cycles. *Quaternary Science Reviews*, 16, 169–185.
Piotrowski, J.A., Larsen, N.K., Menzies, J. & WYSOTA, W. (2006) Formation of subglacial till under transient bed conditions: deposition, deformation, and basal decoupling under a Weichselian ice sheet lobe, central Poland. *Sedimentology*, 53, 83–106.
Piotrowski, J.A. & Tulaczyk, S. (1999) Subglacial conditions under the last ice sheet in northwest Germany: ice-bed separation and enhanced basal sliding? *Quaternary Science Reviews*, 18, 737–751.
Prothro, L.O., Simkins, L.M., Majewski, W. & Anderson, J.B. (2018) Glacial retreat patterns and processes determined from integrated sedimentology and geomorphology records. *Marine Geology*, 395, 104–119.
Reinardy, B.T.I., Hjelstuen, B.O., Sejrup, H.P., Augedal, H. & Jørstad, A. (2017) Late Pliocene-Pleistocene environments and glacial history of the northern North Sea. *Quaternary Science Reviews*, 158, 107–126.
Reinardy, B.T.I., Sejrup, H.P., Hjelstuen, B.O., King, E. & Augedal, H. (2018) A Quaternary aminostratigraphy constraining chronology of depositional environments in the North Sea Basin. *Marine Geology*, 402, 139–152.
Rignot, E., Mouginot, J. & Scheuchl, B. (2011) Antarctic grounding line mapping from differential satellite radar interferometry. *Geophysical Research Letters*, 38, L10504.
Roberts, D.H., Evans, D.J.A., Callard, S.L. et al. (2018a) Ice marginal dynamics of the last British-Irish Ice Sheet in the southern North Sea: Ice limits, timing and the influence of the Dogger Bank. *Quaternary Science Reviews*, 198, 181–207.
Roberts, D.H., Grimoldi, E., Callard, L. et al. (2018b) The mixed-bed glacial landform imprint of the North Sea Lobe in the western North Sea. *Earth Surface Processes and Landforms*, 44, 1233–1258.
Röthlisberger, H. (1972) Water pressure in intra- and subglacial channels. *Journal of Glaciology*, 11, 177–203.
Salamon, T. (2014) Basal till and subglacial conditions at the base of the Upper Odra ice lobe (southern Poland) during the Odranian (Saalian) Glaciation. *Geological Quarterly*, 58, 779–794.
Schmidt, B.E., Washam, P., Davis, P.E.D., Nicholls, K.W., Holland, D.M., Lawrence, J.D. et al. (2023) Heterogeneous melting near the Thwaites Glacier grounding line. *Nature*, 614, 471–478.
Scourse, J.D., Chiverrell, R.C., Smedley, R.K., Small, D., Burke, M.J., Saher, M. et al. (2021) Maximum extent and readvance dynamics of the Irish Sea Ice Stream and Irish Sea Glacier since the Last Glacial Maximum. *Journal of Quaternary Science*, 36, 780–804.
Sejrup, H.P., Aarseth, I., Ellingsen, K.L., Reither, E., Jansen, E., Løvlie, R. et al. (1987) Quaternary stratigraphy of the Fladen area, central North Sea: a multidisciplinary study. *Journal of Quaternary Science*, 2, 35–58.
Sejrup, H.P., Aarseth, I. & Haflidason, H. (1991) The Quaternary succession in the northern North Sea. *Marine Geology*, 101, 103–111.
Sejrup, H.P., Clark, C.D. & Hjelstuen, B.O. (2016) Rapid ice sheet retreat triggered by ice stream debuttressing: Evidence from the North Sea. *Geology*, 44, 355–358.
Sejrup, H.P., Haflidason, H., Aarseth, I., King, E., Forsberg, C.F., Long, D. et al. (1994) Late Weichselian glaciation history of the northern North-Sea. *Boreas*, 23, 1–13.
Sejrup, H.P., Hjelstuen, B.O., Nygård, A., Haflidason, H. & Mardal, I. (2015) Late Devensian ice marginal features in the central North Sea—Processes and chronology. *Boreas*, 44, 1–13.
Sejrup, H.P., Hjelstuen, B.O., Patton, H. et al. (2021) The role of ocean and atmospheric dynamics in the marine-based collapse of the last Eurasian Ice Sheet. *Communications Earth & Environment*, 3, 119.
Siegfried, M.R., Fricker, H.A., Carter, S.P. & Tulaczyk, S. (2016) Episodic ice velocity fluctuations triggered by a subglacial flood in West Antarctica. *Geophysical Research Letters*, 43, 2640–2648.
Stearns, L.A., Smith, B.E. & Hamilton, G.S. (2008) Increased flow speed on a large East Antarctic outlet glacier caused by subglacial floods. *Nature Geoscience*, 1, 827–831.
Stewart, M.A. & Lonergan, L. (2011) Seven glacial cycles in the middle–late Pleistocene of northwest Europe: Geomorphic evidence from buried tunnel valleys. *Geology*, 39, 283–286.
Stoker, M.S., Balson, P.S., Long, D. et al. (2011) An overview of the lithostratigraphical framework for the Quaternary deposits on the United Kingdom continental shelf. *British Geological Survey Research Report*, 48.
Stoker, M.S. & Long, D. (1984) A relict ice-scoured erosion surface in the central North Sea. *Marine Geology*, 61, 85–93.
Svendsen, J.I., Briner, J.P., Mangerud, J. & Young, N.E. (2015) Early break-up of the Norwegian Channel Ice Stream during the Last Glacial Maximum. *Quaternary Science Reviews*, 107, 231–242.
Thornalley, D.J.R., Elderfield, H. & McCave, I.N. (2011) Reconstructing North Atlantic deglacial surface hydrography and its link to the Atlantic overturning circulation. *Global and Planetary Change*, 79, 163–175.
Walder, J.S. & Fowler, A. (1994) Channelized subglacial drainage over a deformable bed. *Journal of Glaciology*, 40, 3–15.
Warburton, K.L.P., Hewitt, D.R. & Neufeld, J.A. (2020) Tidal grounding-line migration modulated by subglacial hydrology. *Geophysical Research Letters*, 47, e2020GL089088.
Weertman, J. (1972) General theory of water flow at the base of a glacier or ice sheet. *Reviews of Geophysics*, 10, 287–333.